

TRANSVERSE POLARIZATION OF BETA PARTICLES  
FROM  
POLARIZED NUCLEI

Thesis by  
John Kevin Markey

In Partial Fulfillment of the Requirements  
for the Degree of  
Doctor of Philosophy

California Institute of Technology  
Pasadena, California

1985

(Submitted February 7, 1985)

to  
Ellen  
and  
Samantha

ACKNOWLEDGMENTS

I wish to thank Professor Felix Boehm for his encouragement and support throughout my studies at Caltech.

I am indebted to Dr. Eric Bovet for invaluable help and advice in my experimental projects.

Thanks are due Dr. Petr Vogel, Professors Charles Barnes and John LoSecco for many enlightening discussions.

The assistance of Herb Henrikson is very appreciated.

The constant assistance and friendship of Mrs. Elsa Garcia is deeply appreciated.

The financial assistance provided by the California Institute of Technology and the U.S. Department of Energy is gratefully acknowledged.

## ABSTRACT

In this thesis an experiment to measure the transverse polarization of electrons from the decay of polarized  $^{60}\text{Co}$  is presented. The result

$$P = ( 1.2 \pm 0.2 ) \gamma \sqrt{1 - v^2/c^2} \frac{\langle \vec{J} \rangle}{J}$$

is consistent with the predicted polarization based on the V - A theory of the weak interaction and the Weinberg, Salam, Glashow model. The theoretical prediction is

$$P = \gamma \sqrt{1 - v^2/c^2} \frac{\langle \vec{J} \rangle}{J}$$

where

$$\gamma = \frac{1}{\sqrt{1 - z^2 \alpha^2}} .$$

This is the first measurement of the transverse polarization of beta particles from the decay of polarized nuclei. The polarization of the electrons was measured by scattering them from gold foil and detecting the scattering asymmetry predicted by Mott scattering theory.  $^{60}\text{Co}$  nuclei were polarized by embedding them in a ferromagnetic host where they feel a strong hyperfine field. The host foil was attached to a dilution refrigerator to lower the entropy of the nuclei and allow for nuclear polarization.



## Chapter 1 INTRODUCTION

### 1.1 THE BETA DECAY WEAK INTERACTION

For many years the weak interaction has been the focus of interest of much of the physics community. In the past the study of its properties has been filled with excitement and new ideas. Recently progress has been made toward the understanding and unification of the fundamental interactions. The discoveries of neutral weak currents<sup>1</sup> and the intermediate vector bosons,  $W$  and  $Z$ ,<sup>2</sup> have solidified the foundation of the Weinberg, Salam, Glashow model<sup>3</sup> unifying the electromagnetic and weak interactions. In this model parity violation is introduced by coupling the intermediate vector boson to quarks or leptons of definite chirality. Thus, the vector - axial-vector form for the weak force supported by studies of muon decay and consistent with nuclear beta decay is a natural consequence.

Since the discovery of parity violation by the weak force<sup>4</sup> the symmetry properties of the fundamental interactions have been central issues. With the discovery of both time reversal and the combination of parity and charge conjugation violation in the weak decays of the neutral K-mesons<sup>5</sup> the investigation of time reversal symmetry has been stimulated. However, unlike the case of parity violation, little progress has been made toward the understanding of time reversal violation. Thus, the study of the time reversal symmetry of fundamental processes with increasingly better accuracy is of great importance in understanding this situation.

Time reversal violation is not predicted by the simplest W.S.G. model. Extensions of the model are needed in order to generate time reversal violation. In the Kobayashi-Maskawa model<sup>6</sup> the matrix describing the weak interaction eigenstates in terms of the quark mass eigenstates for six

quarks can lead to time reversal violation if the mixing parameters have a complex phase. Alternatively, Weinberg<sup>7</sup> and others<sup>8</sup> have proposed additions of extra Higgs bosons to the model other than those needed to give the W and Z their mass. These extra Higgs can generate time reversal violation through their interactions with quarks. This model may soon be in conflict with the experiments on the electric dipole moment of the neutron.

Historically the weak interaction in nuclear beta decay has been described by the most general local Lorentz invariant interaction. The weak Hamiltonian is written<sup>9</sup>

$$H = \frac{G}{\sqrt{2}} \sum_i (\bar{\psi}_p O_i \psi_n) [\bar{\psi}_e O_i (C_i + C'_i \gamma_5) \psi_\nu] + \text{H.C.} \quad (1.1.1)$$

where  $i = S, V, T, A,$  and  $P$ . Here

$$\begin{aligned} O_S &= 1, & O_V &= \gamma_\mu, & O_T &= -\frac{i}{2\sqrt{2}} (\gamma_\mu \gamma_\lambda - \gamma_\lambda \gamma_\mu) \\ O_A &= -i\gamma_\mu \gamma_5, & O_P &= i\gamma_5. \end{aligned} \quad (1.1.2)$$

These are the scalar, vector, tensor, axial-vector, and pseudoscalar interactions corresponding to their Lorentz transformation properties. The so called even and odd coupling constants,  $C_i$  and  $C'_i$ , are in general complex constants. Time reversal symmetry and the combination of parity with charge conjugation will be broken by this interaction if any of the coupling constants have a complex relative phase to the others. Thus, it is required that all constants be real for time reversal invariance to hold. The W.S.G. model predicts the following relations

$$\begin{aligned} C_S, C'_S, C_T, C'_T, C_P, C'_P &= 0, & C_V &= C'_V = 1 \\ C_A &= C'_A, & G &= g \cos \theta_C. \end{aligned} \quad (1.1.3)$$

Here,  $g$  is the universal weak coupling strength and  $\theta_C$  is the Cabibo angle. The axial-vector coupling should differ from minus the vector coupling only due to a renormalization to include interactions with virtual quarks. However, the presence of contributions to nuclear decay by scalar and tensor

interactions has not been experimentally ruled out. Also the restriction to  $C_i = C'_i$  corresponding to purely left handed lepton and quark couplings is not complete. Many different types of experiments have been performed to determine the presence of each of these interactions. The most general fit of the coupling constants to the experimental results for allowed nuclear beta decays has been carried out by Boothroyd, Markey and Vogel.<sup>10</sup> The analysis was restricted to real couplings. The best fit to the data gives

$$\frac{C_A}{C_V} = -1.261, \quad C_A = C'_A, \quad C_V = C'_V$$

with the tensor and scalar terms zero. The limits on the tensor and scalar

interactions are

$$\left| \frac{C_S}{C_V} \right| < 0.23, \quad \left| \frac{C_S}{C_V} \right| < 0.19$$

$$\left| \frac{C_T}{C_A} \right| < 0.09, \quad \left| \frac{C_T}{C_A} \right| < 0.09.$$

These limits are expected to be even weaker if the restriction to real constants is removed. Thus, the contributions to nuclear beta decay by time reversal violating couplings can not be ruled out.

Several types of time reversal tests can be done with nuclei. A well known test is the experimental limit on the presence of a static electric dipole moment of the neutron. The experimental result is<sup>11</sup>

$$d_n < 4 \times 10^{-25} \text{ e-cm (95 \% C.L.)}.$$

Theoretical predictions range from  $10^{-25}$  for the Higgs exchange model<sup>12</sup> to  $10^{-32}$  e-cm for the K.M. model<sup>13</sup> of time reversal violation.

Other tests of time symmetry use measurements of nuclear reaction detailed balance or electromagnetic radiation correlations. The most stringent limit on time reversal violating contributions to nuclear reactions is in the case of<sup>14</sup>



A limit of  $5 \times 10^{-4}$  of the time reversal symmetric amplitudes has been

measured. Time reversal violation may be observed by determining the phase angle between the amplitudes of competing multipoles in a nuclear transition. The best limit on time reversal violating phase was obtained in our laboratory giving<sup>15</sup>

$$\sin \eta < 5 \pm 4 \times 10^{-4}.$$

An experiment has been performed to look for time reversal violation in the decay of polarized positive muons.<sup>16</sup> The resulting limit on the transverse polarization of the positrons lying perpendicular to the plane of the muon spin and the positron momentum is consistent with time reversal symmetry. The limit can be described by a weak interaction of

$$V = (1 + \epsilon) A, \quad |\text{Im } \epsilon| \leq 0.15.$$

For allowed nuclear beta decay the search for time reversal violation is analogous to the measurement of the phase angle between amplitudes for the couplings described above. The general measured correlation parameter will contain contributions of the form

$$\gamma = |A_i| |A_j| e^{i\phi_{ij}}$$

where  $A_i$  and  $A_j$  are the two amplitudes and  $\phi_{ij}$  is the phase angle between them. Many different types of correlations can be measured to restrict the phase angle to the time reversal consistent values of 0 or  $\pi$ . The well known experiment of Wu et al.<sup>17</sup> the beta angular correlation from polarized nuclei, is dependent on the  $\cos(\phi_{ij})$ . In order to do sensitive tests of time reversal symmetry, correlations including the  $\sin(\phi_{ij})$  must be used. This is equivalent to a requirement that the naive symmetry of the correlation be odd with respect to time reversal. For example, the correlation  $\vec{J}_n \cdot \vec{p}_\beta \times \vec{p}_\nu$  has been measured for the decay of polarized neutrons. Under time reversal this becomes

$$(-\vec{J}_n) \cdot (-\vec{p}_\beta) \times (-\vec{p}_\nu) = -(\vec{J}_n \cdot \vec{p}_\beta \times \vec{p}_\nu).$$

This experiment is sensitive to  $\sin(\phi_{AV})$ . In table 1.1.1 is presented the existing experimental results with their correlations and relevant phase angle restrictions.

Our experimental program is directed toward the measurement of

$$\vec{J}_{Co} \cdot \vec{p}_\beta \times \vec{\sigma}_\beta$$

for the decay of polarized  $^{60}\text{Co}$ . This can be achieved by measuring the transverse polarization of the electrons from the decay of the polarized nuclei which lies perpendicular to the plane of the electron momentum and the nuclear polarization.

DECAY	CORRELATION	RESULT	PHASE LIMIT
$n \rightarrow p \ e \ \nu^{18}$	$D \vec{J} \cdot \vec{P}_\beta \times \vec{P}_\nu$	$-0.0011 \pm 0.0017$	$\phi_{AV} = 180.14 \pm 0.22^\circ$
$Ne \rightarrow F \ e \ \nu^{19}$	$D \vec{J} \cdot \vec{P}_\beta \times \vec{P}_\nu$	$0.0004 \pm 0.0008$	$\phi_{AV} = 180.04 \pm 0.09^\circ$
same $^{20}$	$R \vec{J} \cdot \vec{\sigma}_\beta \times \vec{P}_\nu$	$-0.08 \pm 0.05$	$C_S C_A \sin \phi_{SA} = -0.2 \pm 0.1^\circ$
$Co \rightarrow Fe \ e \ \nu^{21}$	$E_1 \vec{J} \cdot (\vec{P}_\beta \times \vec{k}_\gamma) \vec{J} \cdot \vec{k}_\gamma$	$-0.01 \pm 0.02$	$\phi_{AV} = 183 \pm 6^\circ$

Table 1.1.1 Nuclear beta decay time reversal tests

## 1.2 BETA PARTICLE POLARIZATION

The discovery of parity violation in 1957<sup>22</sup> in nuclear beta decay quickly drew attention to the measurement of the polarization of electrons and positrons. As a result of the violation of parity symmetry by the weak interaction beta particles from the decay of unpolarized nuclei are longitudinally polarized. However, the subject of electron polarization predates the discovery of parity violation. The prediction of the spin dependence in the scattering of electrons from nuclei<sup>23</sup> precipitated the study of techniques of producing and measuring the polarization of electrons. Today, the polarization of beta particles provides a valuable tool for the study of the structure of the weak interaction in nuclear beta decay.

In general the polarization of an electron is characterized by a three dimensional unit vector,  $\langle \vec{\sigma} \rangle$ . It corresponds to the direction of the spin of the electron in its rest frame. The electron polarization in a direction  $\hat{n}$  is given by

$$P_{\hat{n}} = \langle \vec{\sigma} \cdot \hat{n} \rangle = \frac{N^+ - N^-}{N^+ + N^-}$$

$N^+$  ( $N^-$ ) is the probability of finding the electron with spin in the direction of  $\hat{n}$  ( $-\hat{n}$ ). For an electron with momentum  $\vec{p}$  in the laboratory it is convenient to define three mutually perpendicular projections of the polarization. In figure 1.2.1 these components are schematically shown. There are two independent transverse polarization projections,  $P_{T_1}$  and  $P_{T_2}$ , along with the longitudinal polarization,  $P_L$ .

Several techniques have been used to measure the longitudinal polarization of beta particles from the decay of unpolarized nuclei. The electron longitudinal polarization has been converted to transverse polarization by the deflection in the radial electric field produced in an electrostatic

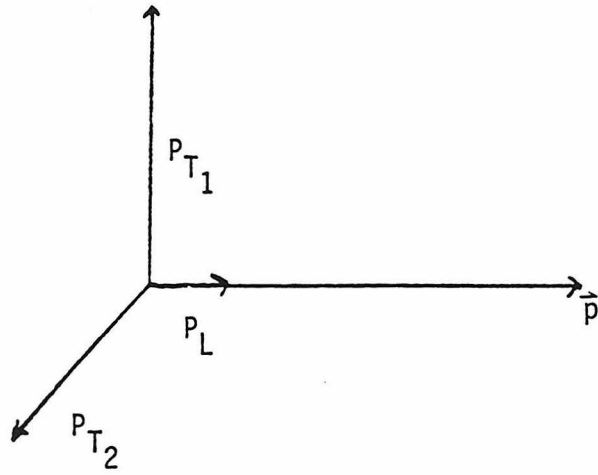


Figure 1.2.1 Polarization projections

spectrometer. The resulting transverse polarization was measured by the scattering asymmetry in Mott scattering from heavy nuclei.

The most sensitive measurements of the longitudinal polarization of positrons from nuclear beta decay detect the change in population of the singlet and triplet positronium states in a strong longitudinal magnetic field. Thus the polarization does not need to be converted to a transverse orientation.

The longitudinal polarization has been measured to be consistent within a few percent of the pure V - A weak interaction predictions. For electrons<sup>24</sup>

$$\text{V - A Theory } P_L = -\frac{v}{c} \quad \text{Experiment } P_L = (-1.01 \pm 0.03) \frac{v}{c}$$

and for positrons<sup>25</sup>

$$\text{V - A Theory } P_L = \frac{v}{c} \quad \text{Experiment } P_L = (0.99 \pm 0.04) \frac{v}{c}.$$

Beta particles from the decay of unpolarized nuclei are not expected to be transversely polarized(it would violate the assumption of the isotropy of space). However, beta particles from the decay of polarized nuclei are expected to be transversely polarized. Tolhoek and de Groot<sup>26</sup> in 1951 described the production of polarized beta particles from the decay of polarized nuclei based only on the conservation of angular momentum. This polarization would be in the direction of the nuclear polarization. Thus, beta particles emitted perpendicular to the nuclear polarization should be transversely polarized with a polarization  $P_{\perp}$ . Depicted in figure 1.2.2 are the relative orientations of the beta particle spin, momentum and the nuclear polarization. In addition to the component  $P_{\parallel}$ , there is another transverse polarization component,  $P_{\perp}$ . The presence of a non-zero value for  $P_{\perp}$  is equivalent to the existence of a correlation of the form in the beta particle distribution for the decay of polarized nuclei. As discussed in section 1.1 this might signal a violation of time reversal symmetry

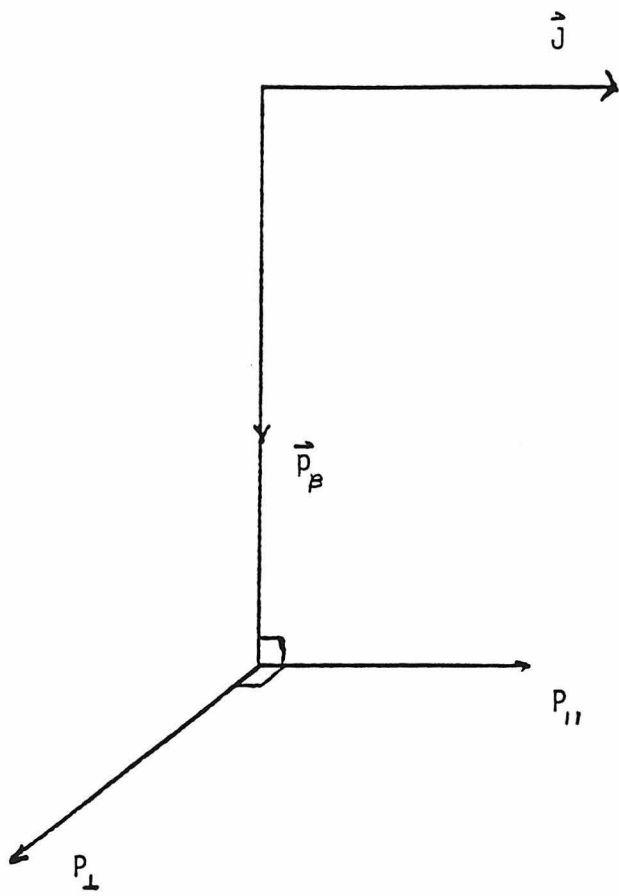


Figure 1.2.2 Nuclear and beta particle polarization

by the weak interaction in beta decay. However, because of the influence of the nuclear charge,  $Z$ , on the beta particle as it leaves the nucleus there is expected to be a correlation of this form even if the beta decay weak interaction has no time reversal violating couplings. A detailed presentation of the expected transverse polarizations, both parallel and perpendicular to the nuclear polarization, will be given in the next chapter.

There has been only a single previous experiment to measure the transverse polarization of beta particles from the decay of polarized nuclei. An upper limit<sup>27</sup>

$$P_{\perp} \leq 0.01$$

on the transverse polarization,  $P_{\perp}$ , of positrons from the decay of polarized <sup>19</sup>Ne is consistent with time reversal symmetry. In this case the value of  $P_{\perp}$  from nuclear charge interactions is on the order of  $10^{-3}$ . The expected  $P_{\parallel}$  of about  $10^{-2}$  was not measured.

The eventual goal of the experiments discussed in this thesis is the measurement of possible contributions to the correlation described by

$$\hat{J}_{Co} \cdot \hat{p}_{\beta} \times \hat{\sigma}_{\beta}$$

from time reversal violating weak interaction couplings in nuclear beta decay. As the first step toward the measurement of  $P_{\perp}$  for beta particles from the decay of polarized nuclei this thesis describes the first measurement of  $P_{\parallel}$ . Polarized 60-Co was produced at low temperature utilizing the interaction of the nuclear magnetic moment with the hyperfine magnetic field in a ferromagnetic host material. The transverse polarization,  $P_{\perp}$  of the electrons emitted perpendicular to the nuclear polarization was

measured by Mott scattering the electrons from gold foil. The results are

$$\text{Experiment } P_{\parallel} = ( 1.2 \pm 0.2 ) \gamma \sqrt{1 - v^2/c^2} \frac{\langle J_{\parallel} \rangle}{J}$$

Here, the theoretical prediction is based on a pure V - A weak interaction.

## Chapter 2 THE PRINCIPLES OF THE EXPERIMENT

### 2.1 NUCLEAR POLARIZATION AT LOW TEMPERATURE

Nuclear polarization is the preferential ordering of nuclear angular momenta, or spins, in space. An example would be the orientation of nuclear spins along an axis of quantization. The quantization of angular momentum determines states with different projections of angular momentum on this axis. Nuclear polarization occurs when the states with a positive projection of the angular momentum are populated unequally to the states with a negative projection of the angular momentum. This may be achieved for an ensemble of nuclei with spin  $J$  if the energy degeneracy of the  $2J + 1$  states is removed by an external influence and the entropy is dramatically decreased, typically by the transfer of energy to another system at low temperature.

The orientation of a system of nuclei with rotational symmetry about an arbitrary axis can be completely characterized by the relative populations  $p(m)$  of the states with an angular momentum projection,  $m$ , on this axis. The  $p(m)$  are normalized according to

$$\sum_m p(m) = 1.$$

The nuclear polarization along this axis is equal to

$$\frac{\langle \vec{J} \rangle}{J} = \frac{1}{J} \sum_m m p(m).$$

It is convenient to define orientation parameters,  $B_\lambda$

to characterize the distribution of  $p(m)$  where

$$B_\lambda \equiv \left[ (2\lambda + 1)(2J + 1) \right]^{1/2} \sum_m (-1)^{m+J} \begin{pmatrix} J & J & \lambda \\ -m & m & 0 \end{pmatrix} p(m).$$

Here

$$\begin{pmatrix} J & J & \lambda \\ -m & m & 0 \end{pmatrix}$$

is a Wigner 3-J symbol. The  $B_\lambda$  vanish for  $\lambda > 2J$ . The nuclear polarization is related to  $B_\lambda$  by

$$\frac{\langle \bar{J} \rangle}{J} = B_1 \frac{J+1}{3J} .$$

The interaction between the nuclear magnetic dipole moment,  $\mu$ , and the hyperfine magnetic field,  $H$ , will facilitate orientation of the nuclei by removing the degeneracy of the different  $m$  states. The interaction energy is described by the Hamiltonian

$$H = - \hat{\mu} \cdot \hat{H} .$$

The state populations become

$$p(m) = e^{m\mu H/KTJ} \frac{1}{\sum_m e^{m\mu H/KTJ}} .$$

To produce substantial polarization a large value of the Boltzmann factor

$$\mu H/KT$$

is required.

Besides removing the degeneracy of the spin states the entropy of the system of nuclei must be reduced. The entropy of the nuclei was lowered by thermally linking them to a  $He^3$ - $He^4$  dilution refrigerator. The refrigerator is capable of sustaining 20mK temperature with a small heat load.

The general angular distribution of radiation emitted by oriented nuclei at an angle  $\Theta$  from the axis of orientation is<sup>28</sup>

$$W(\Theta) = \sum_\lambda B_\lambda U_\lambda A_\lambda Q_\lambda P_\lambda(\cos \Theta)$$

$P_\lambda$  is the Legendre polynomial of order  $\lambda$ . The deorientation coefficient  $U_\lambda$  corrects for the effect of unobserved radiation emitted by the nucleus prior to the emission of the radiation described by  $W(\Theta)$ . The angular distribution coefficients  $A_\lambda$  are determined by the properties of the particular radiation. Corrections for the finite solid angles subtended by the source and detector are by the  $Q_\lambda$ .

The nuclear polarization achieved in this experiment was found by considering the spatial distribution of gamma ray emission from the nuclei. The gamma ray angular distribution for pure E2 gamma ray radiations is

$$W_{\gamma}(\theta) = 1 + \sum_{K=2,4} B_K U_K A_K Q_K P_K(\cos \theta).$$

The rate of gamma ray emission at 90 degrees was monitored continuously during the experiment. The nuclear orientation parameters  $B_2^{mK}$  and  $B_4^{mK}$  for the polarized nuclei at mK temperature were determined by the measured change,

$$\Delta = \frac{W_{\gamma}(90^{\circ}) \text{ at mK}}{W_{\gamma}(90^{\circ}) \text{ at LHe}} = 1 + B_2^{mK} U_2 A_2 Q_2 P_2(0) + B_4^{mK} U_4 A_4 Q_4 P_4(0).$$

in the gamma ray distribution. The  $B_2$  and  $B_4$  terms in  $W(90^{\circ})$  at liquid He temperature contribute less than .01 percent to the denominator of  $\Delta$ . They are ignored in this experiment. For an assembly of nuclei with spin  $J$  at a particular temperature, measurement of  $B_2$  and  $B_4$  allows the calculation of  $B_1$ , which is proportional to  $\langle \vec{J} \rangle / J$ , the nuclear polarization.

## 2.2 BETA PARTICLE DISTRIBUTION FROM POLARIZED NUCLEI

The polarization of beta particles from the decay of oriented nuclei is determined by the relative probabilities of beta emission with particular spin and momentum directions. The beta decay distribution for allowed beta decay from oriented nuclei in angle and beta polarization is<sup>29</sup>

$$W dE d\Omega \propto dE d\Omega \left\{ 1 + \frac{\vec{p}}{E} \cdot \left( A \frac{\langle \vec{J} \rangle}{J} + G \vec{\sigma} \right) + \vec{\sigma} \cdot \left( N \frac{\langle \vec{J} \rangle}{J} + Q \frac{\vec{p}}{E+m} \left( \frac{\langle \vec{J} \rangle}{J} \cdot \frac{\vec{p}}{E} \right) + R \frac{\langle \vec{J} \rangle}{J} \times \frac{\vec{p}}{E} \right) \right\}. \quad (2.2.1)$$

$p$  and  $E$  are the momentum and total energy of the beta particle in units with  $c = \hbar = 1$ . The beta particle momentum and spin correlation coefficients,  $A$ ,  $G$ ,  $N$ ,  $Q$ , and  $R$ , are calculated in terms of the weak interaction described in section 1.1, and the Fermi,  $\int 1$ , and Gamow-Teller,  $\int \sigma$ , nuclear matrix elements. Included are the electromagnetic contributions due to the interaction of the beta particle with the nuclear charge,  $Z$ . It is assumed that the  $C_i$  and  $C'_i$  weak coupling constants are equal. Thus, the formulas for the coefficients will be written using  $C_i = C'_i = i$  for  $i = S, A, V, T$ . This corresponds to a weak interaction which couples to purely left handed neutrinos (eigenstates of chirality with negative eigenvalue). The general expressions for the coefficients without this assumption can be found in Jackson, Treiman, and Wyld.<sup>29</sup> However, a removal of this assumption does not alter the main ideas of this section. The assumption only serves to reduce the number of phase angles defined below to a more manageable number. The vector weak coupling will be used to define the positive real axis. The other complex couplings are defined with a phase angle relative to the vector coupling. The correlation coefficients for electron beta decay become

$$\xi_A = \int \sigma \int^2 \lambda \{ 2(T^2 - A^2) + 4\alpha Z \frac{m}{p} TA \sin(\phi_T - \phi_A) \} +$$

$$2 \int \sigma \int^1 \sqrt{\frac{J}{J+1}} \{ 2ST \cos(\phi_S - \phi_T) - 2VA \cos \phi_A + 2\alpha Z \frac{m}{p} (SA \sin(\phi_S - \phi_A) + VT \sin \phi_T) \}$$

$$\xi_G = \int \sigma \int^1 \{ 2(S^2 - V^2) + 4\alpha Z \frac{m}{p} SV \sin \phi_S \} +$$

$$\int \sigma \int^2 \{ 2(T^2 - A^2) + 4\alpha Z \frac{m}{p} TA \sin(\phi_T - \phi_A) \}$$

$$\xi_N = \int \sigma \int^2 \lambda \{ \gamma \frac{m}{E} (2T^2 + 2A^2) + 4TA \cos(\phi_T - \phi_A) \} +$$

$$2 \int \sigma \int^1 \sqrt{\frac{J}{J+1}} \{ 2SA \cos(\phi_S - \phi_A) + 2VT \cos \phi_T + 2\gamma \frac{m}{E} (ST \cos(\phi_S - \phi_T) + VA \cos \phi_A) \}$$

$$\xi_Q = 2 \frac{E - \gamma m}{E - m} \int \sigma \int^2 \lambda \{ T^2 + A^2 - 2TA \cos(\phi_T - \phi_A) \} -$$

$$\int \sigma \int^1 \sqrt{\frac{J}{J+1}} \{ 4SA \sin(\phi_S - \phi_A) + 4VT \sin \phi_T - 4\alpha Z \frac{m}{p} (ST \sin(\phi_S - \phi_T) + VA \sin \phi_A) \}$$

$$\xi_R = \int \sigma \int^2 \lambda \{ 2TA \sin(\phi_T - \phi_A) - 2\alpha Z \frac{m}{p} (T^2 - A^2) \} +$$

$$\int \sigma \int^1 \sqrt{\frac{J}{J+1}} \{ 2SA \cos(\phi_S - \phi_A) + 2VT \cos \phi_T - 2ST \cos(\phi_S - \phi_T) - 2VA \cos \phi_A \}$$

$$\xi = \int \sigma \int^1 \{ 2S^2 + 2V^2 \} + \int \sigma \int^2 \{ 2T^2 + 2A^2 \}, \quad \gamma = \sqrt{1 - \alpha^2 Z^2} \quad . \quad (2.2.2)$$

$$\begin{aligned} \text{Here,} \quad &= 1 && \text{for } J_{\text{final}} = J_{\text{initial}} - 1 \\ \lambda &= \frac{1}{J+1} && \text{for } J_{\text{final}} = J_{\text{initial}} \\ &= \frac{J}{J+1} && \text{for } J_{\text{final}} = J_{\text{initial}} + 1 \end{aligned}$$

where  $J_{\text{initial}}$  is the spin of the beta decaying nucleus and  $J_{\text{final}}$  is the final spin of the nucleus.

As discussed in section 1.1 the weak interaction would violate time reversal symmetry if any of the coupling phase angles are not zero or pi. Therefore, any of these correlations can be altered by a violation of time reversal symmetry. The eventual goal of these experiments with oriented nuclei is to measure the possible contributions to beta decay correlations from scalar couplings with a time reversal violating phase. The correlations most sensitive to a time reversal violating scalar coupling contain terms with  $SA \sin(\phi_S - \phi_A)$  or  $SV \sin(\phi_S)$ . These are A, G, and R. However, the correlation determined by R has a contribution proportional to the  $SA \sin(\phi_S - \phi_A)$  that is not reduced by the electromagnetic factor  $\propto Z$ . Thus, the goal becomes a measurement of the correlation generated by R.

The polarization of beta particles from the decay of polarized nuclei can be calculated using the decay distribution equation 2.2.1. The transverse polarization of beta particles emitted perpendicular to the nuclear polarization has two projections shown in figure 1.2.2 . These become

$$\begin{aligned} P_{\parallel} &= N \frac{\langle J \rangle}{J} \\ P_{\perp} &= R \frac{v}{c} \frac{\langle J \rangle}{J} (\hat{J} \times \hat{p}) \quad . \end{aligned}$$

Here,  $v / c$  is the velocity of the beta particle divided by the speed of light.  $\hat{J}$  and  $\hat{p}$  are unit vectors. R is proportional to the transverse polarization perpendicular to the nuclear polarization,  $P_{\perp}$  . However, the transverse polarization parallel to the nuclear spin,  $P_{\parallel}$ , will be present. As

a first step in developing an experiment to measure  $P_{\perp}$  the measurement of  $P_{\parallel}$  has been achieved. The measurement of  $P_{\perp}$ , and thus R, may simply require a rotation of the polarization detection device by 90 degrees about the initial beta particle momentum vector.

For a time reversal symmetric weak interaction with only vector and axial vector couplings the N and R coefficients become

$$R = \alpha Z \frac{E}{p} N = \alpha Z \frac{m}{p} \frac{|\sigma/\lambda|^2 A^2 + 2 \int \sigma \int_1 \sqrt{\frac{J}{J+1}} VA}{|\int_1|^2 v^2 + |\sigma/\lambda|^2 A^2}$$

A time reversal violating scalar coupling would modify R for mixed Fermi-Gamow-Teller beta transitions by a term containing  $SA \sin(\phi_S - \phi_A)$ . Using the relation of equation 2.2.5 N is generally larger than R. Thus,  $P_{\parallel}$  is expected to be larger than  $P_{\perp}$ .

In this experiment  $P_{\parallel}$  is measured as a function of energy for negative beta particles from the decay of nuclei polarized at low temperature.

### 2.3 MEASUREMENT OF TRANSVERSE POLARIZATION BY MOTT SCATTERING

Several methods are available for measuring the polarization of electrons. The direct measurement techniques take advantage of the dependence of scattering cross-sections on polarization. At high energy, greater than about 1 MeV, Moller scattering from the polarized electrons in magnetically saturated ferromagnetic foils has been used.<sup>30</sup> Here, the polarization sensitivity suffers greatly because only 2 of every 26 target electrons in the target foil are aligned. For energies below 500 keV Mott scattering from high Z nuclei has been used successfully to measure transverse polarization.<sup>31</sup> The spin orbit interaction between the electron magnetic moment and the magnetic field seen in the electron rest frame produced by the motion of the nuclear charge causes the cross section to be strongly spin dependent at large scattering angles.

The first relativistic quantum theory of electron scattering by nuclei predicted the transverse polarization of initially unpolarized electrons after scattering. The spin orientation is perpendicular to the plane of scattering. The amount of polarization,  $S(\theta)$ , is a function of energy and increases approximately linearly with Z. In figure 2.3.1  $S(\theta)$  is plotted for 150 Kev electrons.  $S(90)$  as a function of energy is in figure 2.3.2.

If electrons are initially transversely polarized with polarization P, the scattering cross-section for Mott scattering from nuclei is asymmetric.

$$\frac{d\sigma}{d\Omega} = \frac{d\sigma_p}{d\Omega} \{ 1 - P S(\theta) \sin \phi \} \quad (2.3.1)$$

where  $\frac{d\sigma_p}{d\Omega}$  is polarization independent. Here  $\phi$  is the azimuthal angle of scattering relative to the plane of the initial momentum and the polarization of the electrons. A measurement of the scattering asymmetry yields P. The largest asymmetry is in the plane perpendicular to the initial momentum and the polarization vector ( $\phi = 90$  or  $270$  degrees).

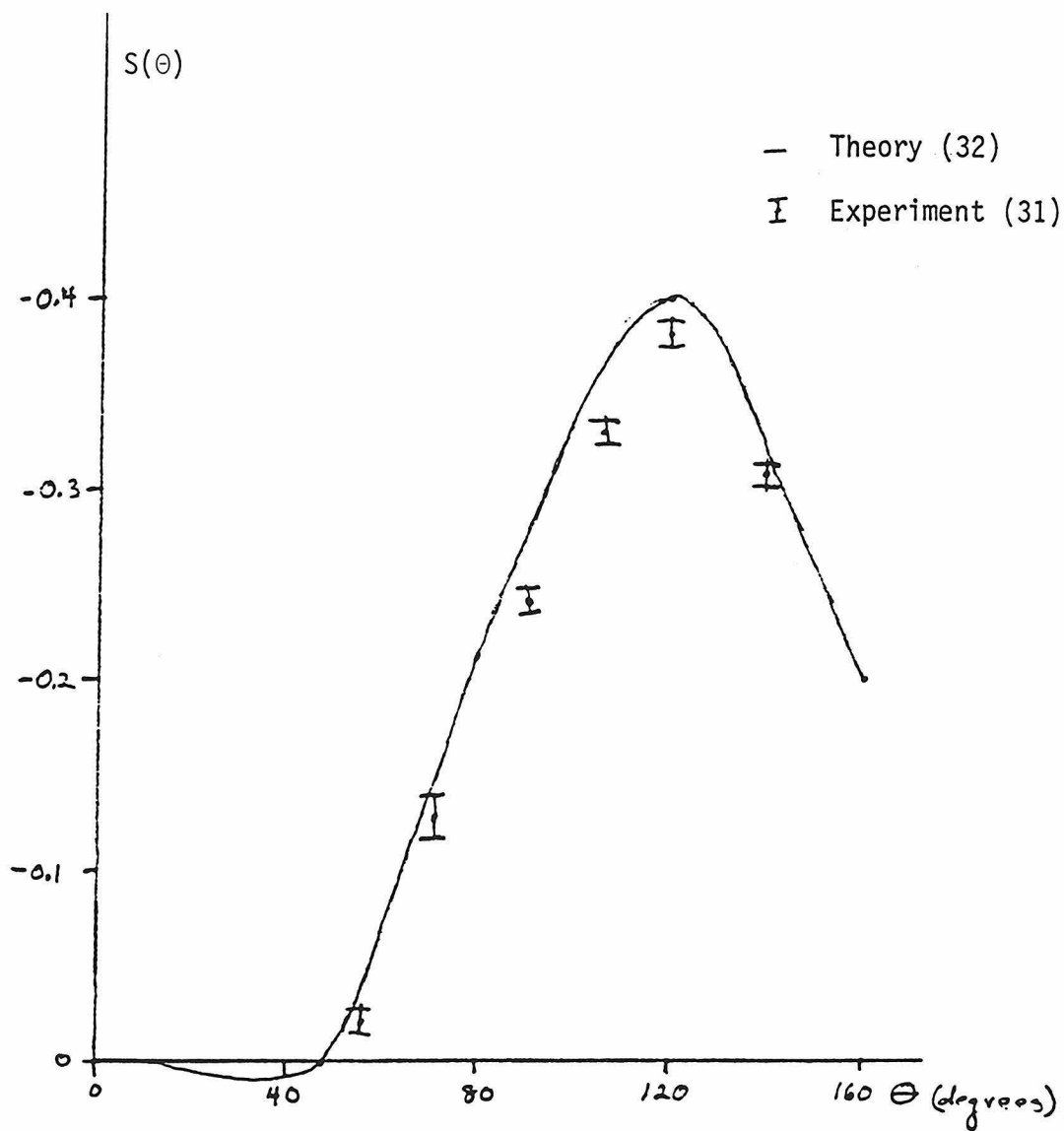


Figure 2.3.1 Mott scattering polarization sensitivity for 150 keV electrons as a function of angle

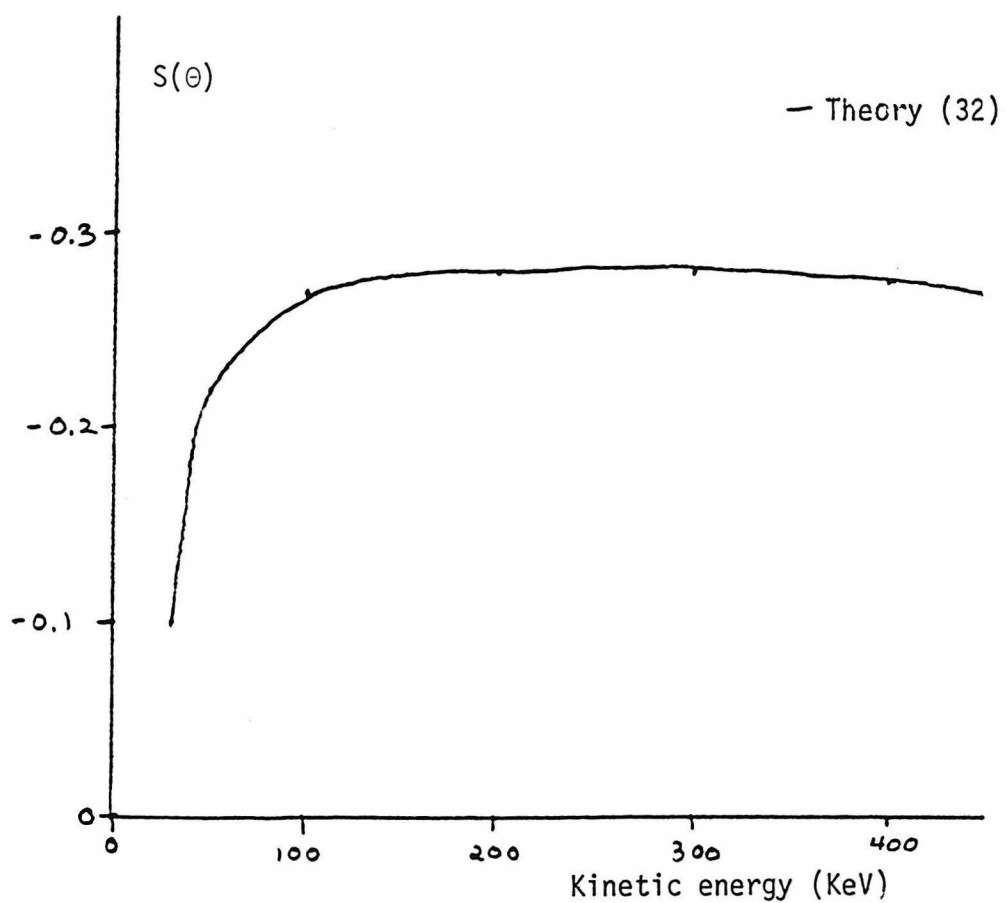


Figure 2.3.2 Mott scattering polarization sensitivity at  $90^\circ$  as a function of electron energy

This is usually denoted as the left-right asymmetry

$$A_S = \frac{L - R}{L + R} = P S(\theta) . \quad (2.3.2)$$

Left is the direction of P crossed into the momentum.

For most experiments equation 2.3.2 does not represent a valid measurement of P . The measured asymmetry,  $A_M$ , is the sum of  $A_S$  and the systematic instrumental asymmetry,  $A_I$ ,

$$A_M = A_S + A_I \quad (2.3.3)$$

$A_I$  is generally due to unequal solid angles or unequal detection efficiencies for the two scattering directions, L and R. In many experiments the separate contributions to  $A_M$  of  $A_S$  and  $A_I$  can be found by measuring  $A_M$  while reversing the direction of P. Also, exchanging the roles of the R and L detectors by rotating the set of detectors around the initial momentum direction by 180 degrees has been used to eliminate the effects of  $A_I$  .

In order to measure the transverse polarization of the electrons in this experiment the scattering asymmetry is measured for the polarized electrons. It is compared with the asymmetry for electrons with the polarization turned off.

$$A_M = \frac{(L - R)_p - (L - R)_{p=0}}{(L + R)_p + (L + R)_{p=0}} = P \cdot E_p \quad (2.3.4)$$

Here, the instrumental asymmetries are removed explicitly.  $E_p$  is the polarization detection efficiency of the polarimeter. The  $E_p$  is a function of the solid angles, detector responses, and  $S(\theta)$  .

In practice the measured  $S(\theta)$  is less than that predicted, by the nuclear scattering cross-section. Plural and multiple scattering in target foils of finite thickness can reduce the efficiency for polarization measurements significantly. The effective S including the reduction due to foil thickness has been measured by several experimenters . Figure 2.3.3 shows the measured  $S(t)$  normalized by S from extrapolating to zero foil thickness. In

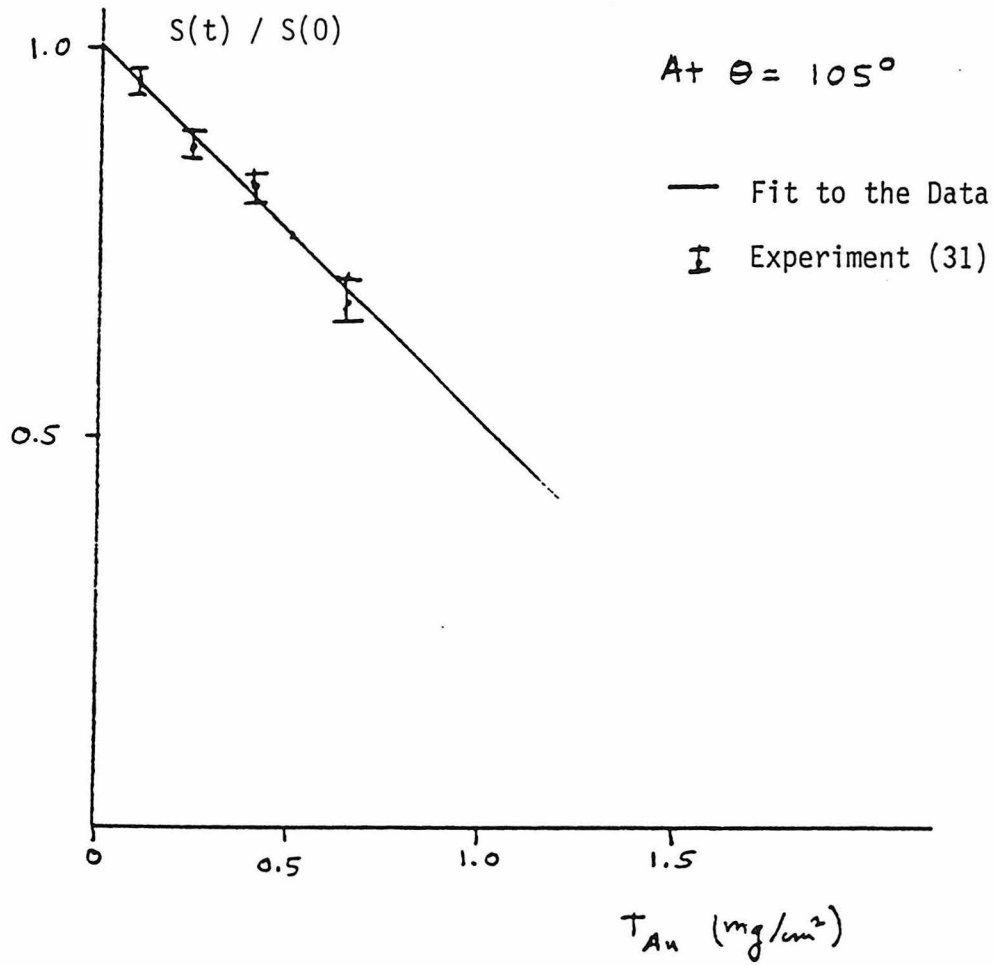


Figure 2.3.3 Mott scattering polarization sensitivity for finite thickness scattering foils normalized to zero thickness foils

this experiment  $S(\theta)$  derived from theoretical calculations<sup>32</sup> corrected for the effects of multiple scattering as determined by previous experimenters' results will be used to calculate  $E_p$ .

The optimal design for a polarimeter to measure transverse polarization must take into consideration the choice of the scattering angles, solid angles, and foil thickness.

## Chapter 3 THE 60 - CO EXPERIMENT

### 3.1 THE CHOICE OF BETA DECAY TRANSITION

In order to test the theory for the transverse polarization of beta particles from polarized nuclei a transition with a large value for  $N$ , in equation 2.2.1, is desired. From the formula for  $N$ , this is satisfied best by a beta transition with  $J_{\text{final}} = J_{\text{initial}}$ , and low energy. To obtain high polarization sensitivity from the Mott scattering technique the beta decay should be an electron decay with a maximum kinetic energy of several hundred keV. To simplify the analysis of experimental results a nucleus with only a single allowed decay in the beta energy region of interest is preferred. Nuclear polarization is made possible by large values for the nuclear magnetic moment and magnetic hyperfine field in a ferromagnetic host. In addition subsequent gamma decay with known properties in the decay scheme of the nuclei is required to measure the nuclear polarization during the experiment. With these criteria in mind 60-Co is a natural choice for the beta decay transition.

The decay scheme of 60-Co is shown in figure 3.1.1 . The two gamma decays are known to be pure E2 by the consistency of their conversion coefficients with predictions.<sup>33</sup> The magnetic moment of 60-Co is from ESR measurements  $\mu = 3.81 \pm 0.01$ <sup>34</sup> and the magnetic hyperfine field in permen-dure, the ferromagnetic host, was found to be  $-282 \pm 4$  KG by NMR(ON).<sup>35</sup> These values result in  $H / Jk = 7.86 \pm 0.11$  mK for the Boltzmann factor. Thus significant nuclear orientation can be obtained at temperatures of about 40 mK.

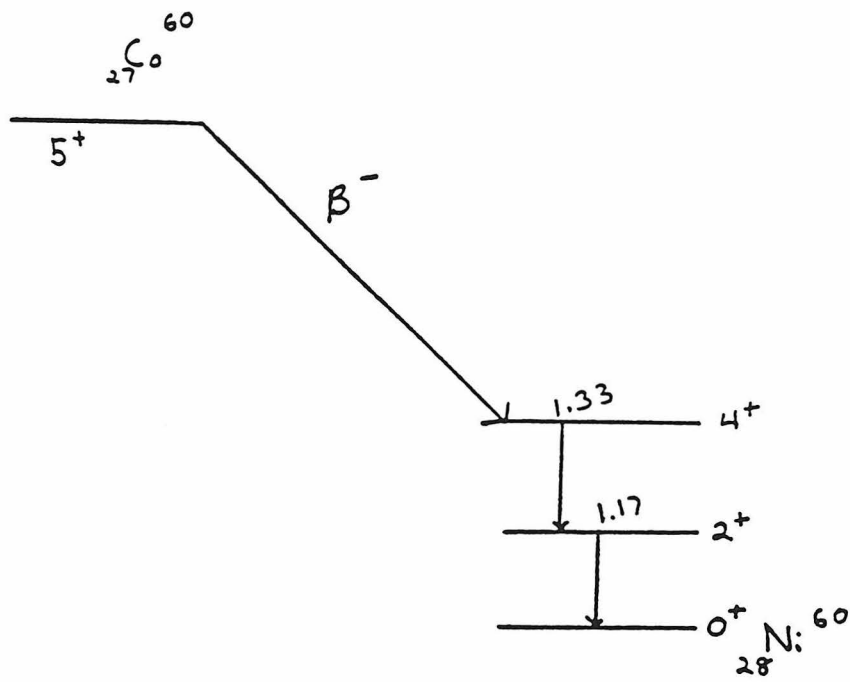


Figure 3.1.1  $^{60}\text{Co}$  decay scheme

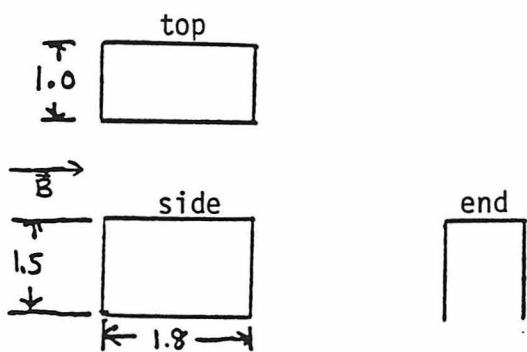
### 3.2 THE PREPARATION OF THE SOURCE

The preparation of the source is crucial to the success of this experiment. In order to minimize the deflection of the momentum and spin of the electrons by the external magnetic field used to saturate the source foil, permendure, an alloy of 49% Fe, 49% Co, and 2% V was used as the host material. Permendure properly heat treated in an external magnetic field is highly anisotropic and can be magnetically saturated along the preferred axis by less than one Oersted.<sup>36</sup> Additionally,  $^{60}\text{Co}$  is not an impurity in permendure and sees a single hyperfine field,  $282 \pm 4$  KG mentioned above, measured in a similar source.

To avoid multiple scattering of the observed beta particles the  $^{60}\text{Co}$  must be diffused into the permendure host as near the foil surface as possible. However, the standard prescription for heat treating permendure requires temperatures of 820 to 850 degrees C for 4 to 24 hours. Such a procedure would result in diffusion of the  $^{60}\text{Co}$  throughout the host. A technique has been developed to resolve this conflict. The host foil is first prepared in the standard fashion. The  $^{60}\text{Co}$  is then applied to the surface and a short diffusion is performed.

The sources used in the experiment were made with 13 micro m thick non-heat-treated permendure foil obtained from Arnold Engineering Co. of Marengo, Ill. The foil was cut and bent into the form shown in figure 3.2.1 . The magnetic properties of the foil were achieved by heat treating it in a pure  $\text{H}_2$  atmosphere with a 140 Orsted external field applied as shown. Figure 3.2.2 gives the first heat treating cycle. The B - H curve of a foil prepared in this way is shown in figure 3.2.3 .

For making these sources  $^{60}\text{Co}$  in 0.1 N HCl was bought from Isotope products in Burbank, Ca., with a specific activity of 380 Ci/ g Co ( pure  $^{60}\text{Co}$  -



dimensions are in centimeters

Figure 3.2.1 Source foil geometry

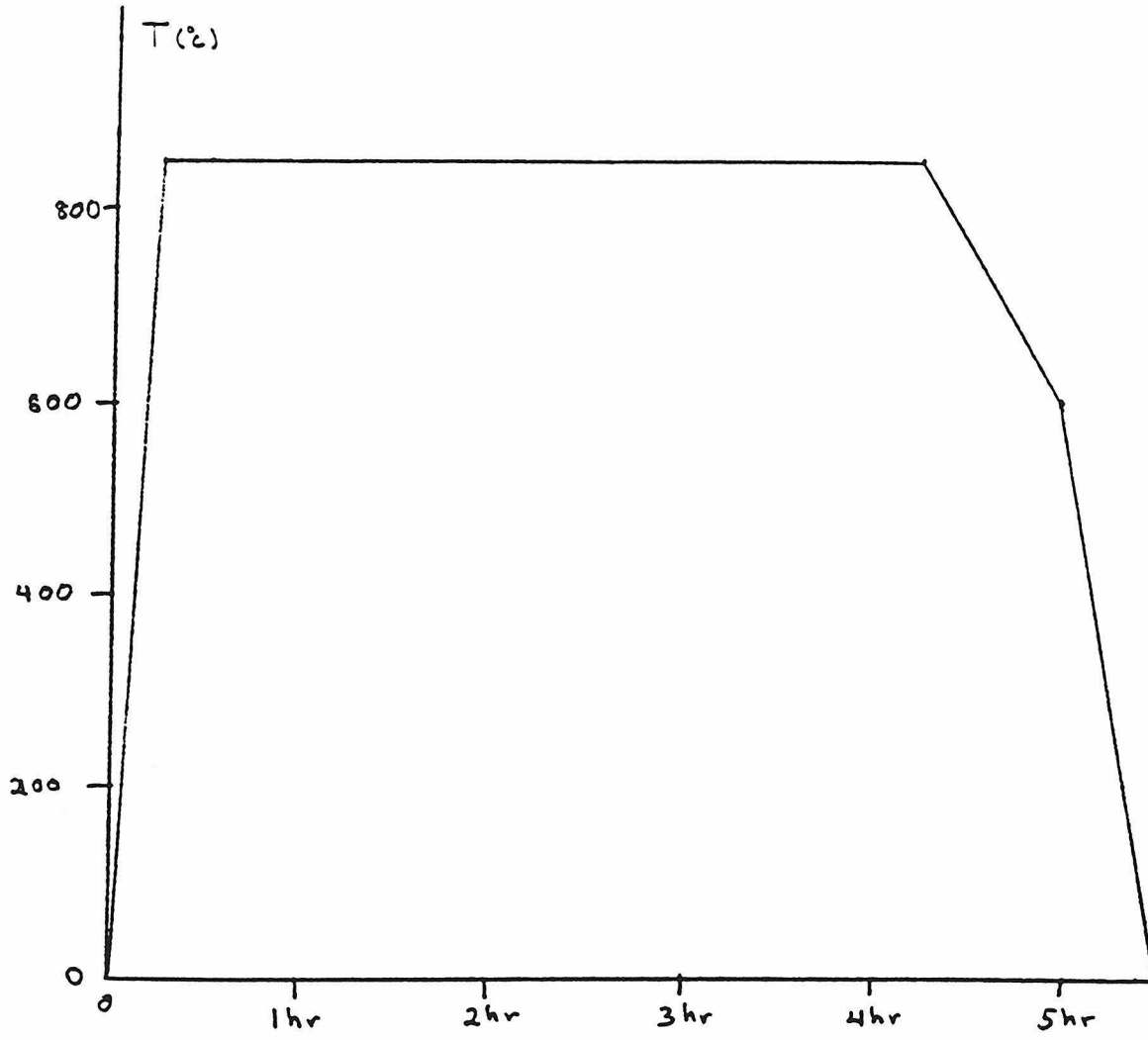


Figure 3.2.2 1st heat treatment cycle for Permendure foil

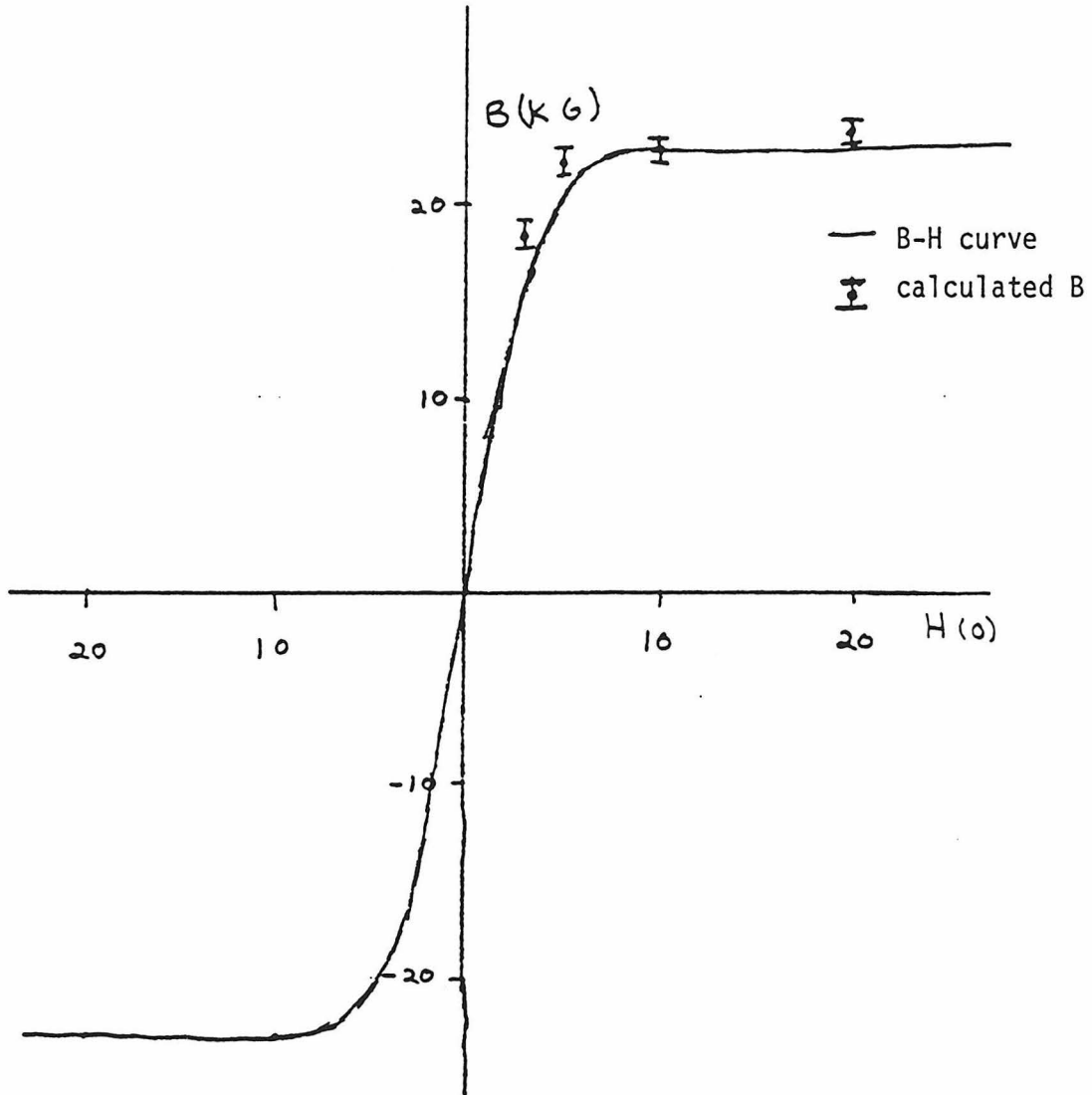


Figure 3.2.3 B - H curve of Permendure source foil

Co is 1100 Ci/ g Co ). Two sources both of about 50 micro Ci were used in this experiment. A drop of 3 mm diameter and 1.5 micro liters of CoCl solution was placed on the the surface of the foil. The acid and water were dried under a small lamp in an argon atmosphere. Also under an argon atmosphere the tabs of the foil were electroplated with nickel. The foil was heat treated the second time for a short period as shown in figure 3.2.4 . The first source with activity of 65 micro Ci was kept at 830 degrees C for 5 minutes. The secound source with an activity of 50 micro Ci was kept at 830 degrees C for 12 minutes. Afterward the surface of each foil was cleaned with cerium oxide and freon to remove any activity remaining unsited on the surface. Typically 80 to 90 percent of the 60-Co dried onto the surface was diffused into the foil.

The magnetic properties of a foil prepared by this technique differed very little from those of a foil treated in the standard way. Figure 3.2.3 includes the B - H curve for a foil after this secund treatment. In addition, the calculation of the saturation of the hyperfine field from the measured gamma ray anisotropy as a function of applied external magnetic field for the first source at 45 m K degrees is shown.

The apparent saturation of these foils at about 10 Orsted instead of the aforementioned less than 1 Orsted can be understood by considering the demagnetizing field for the particular foil geometry. Inside the foil the demagnetizing magnetic field apposes the applied field. The field can be approximately calculated for the center of the foil by

$$H_D = \frac{2 B_s W t}{\pi l^2} = 6 \text{ Oe} .$$

$B_s = 23 \text{ KG}$  is the saturation magnetization,  $l = 1.8 \text{ cm}$  is the length of the foil,  $t = 13 \text{ micro m}$  is the thickness and  $W = 1 \text{ cm}$  is the width of the foil. To saturate the foils in this experiment the demagnetizing field must be

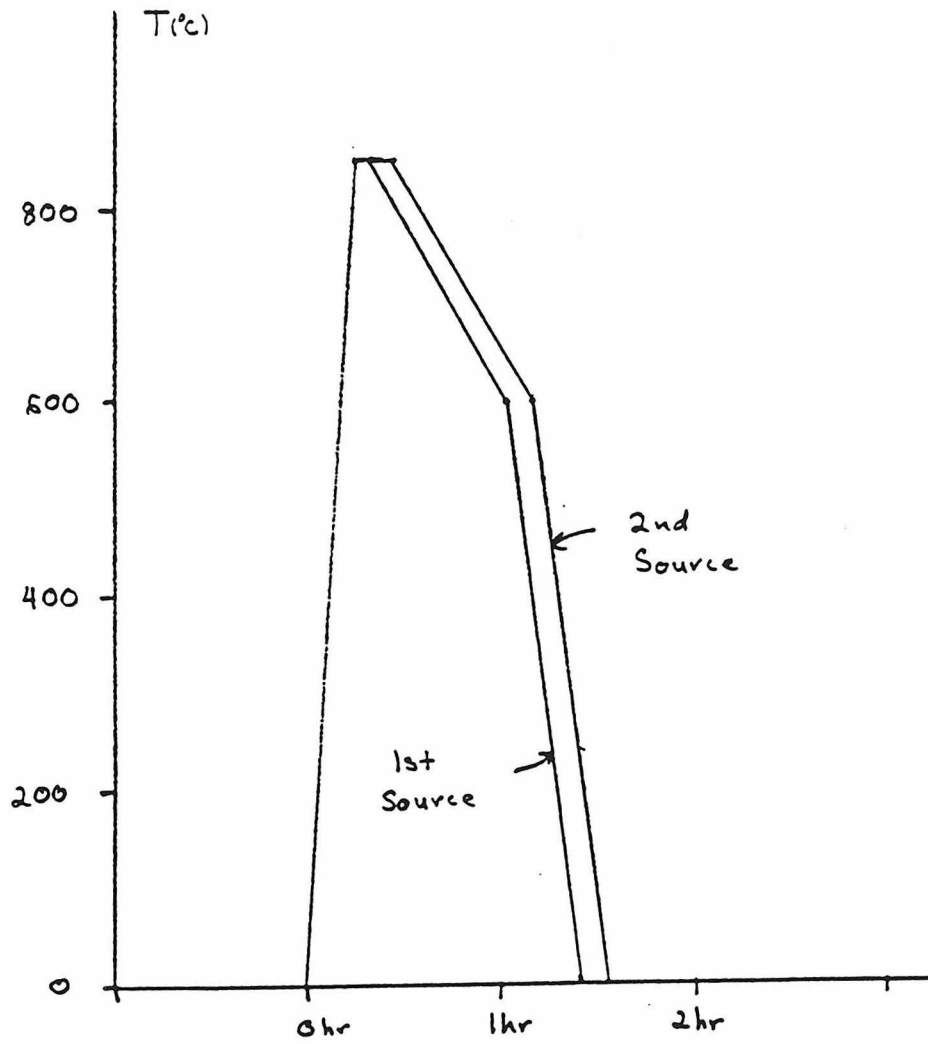


Figure 3.2.4 2nd heat treatment cycle for Permendure foil

overcome by the external applied field.

An estimate of the depolarization due to the multiple scattering in the foil of the observed beta particles will require knowledge of the depth in the foil of the  $^{60}\text{Co}$  diffused through the surface. The distribution was determined by uniformly lapping the surface away. The weight and activity of the foil were measured at steady intervals. In figure 3.2.5 are the resulting depth distributions for the two sources.

The installation of the source into the dilution refrigerator system is quite simple. Figure 3.2.6 shows the geometry of the source and cold finger with respect to the mixing chamber (the coldest part of the refrigerator). After heat treatment the tabs of the source are gold electroplated in an argon atmosphere. The tabs are pressed to the cold finger with the sharp edges of the cold finger clamps. The cold finger is made of OFHC copper and is gold electroplated just before installing the source foil. The foil cold welds to the cold finger at the edges of the clamps. These procedures were necessary to ensure good thermal contact between the foil and the refrigerator.

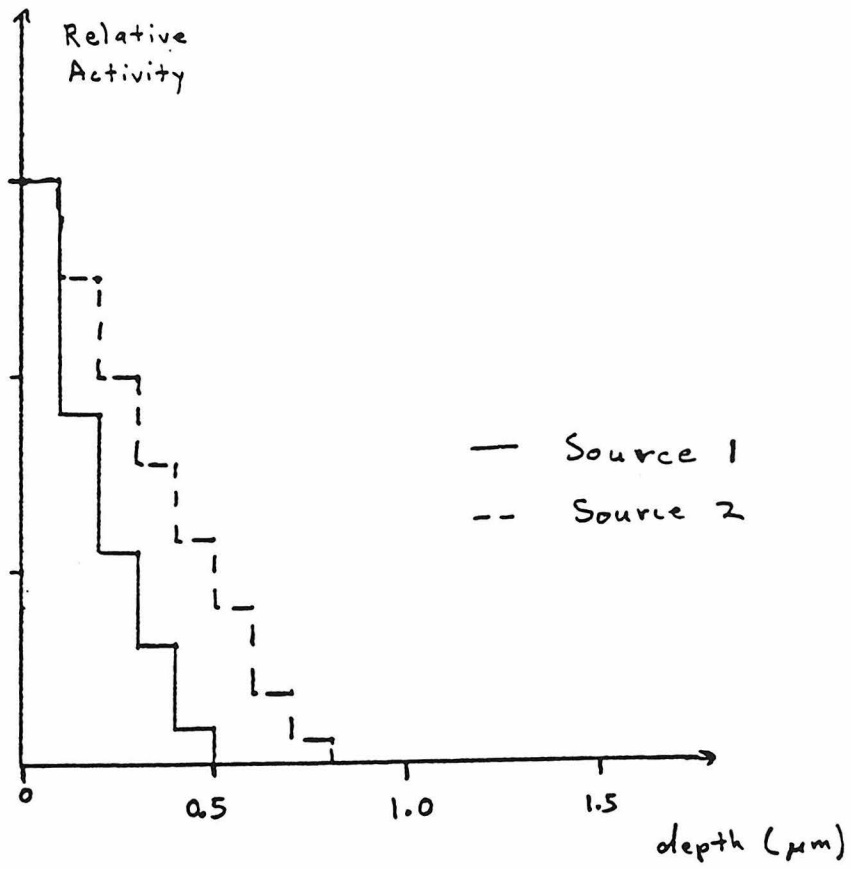


Figure 3.2.5 Activity distribution in the source foils

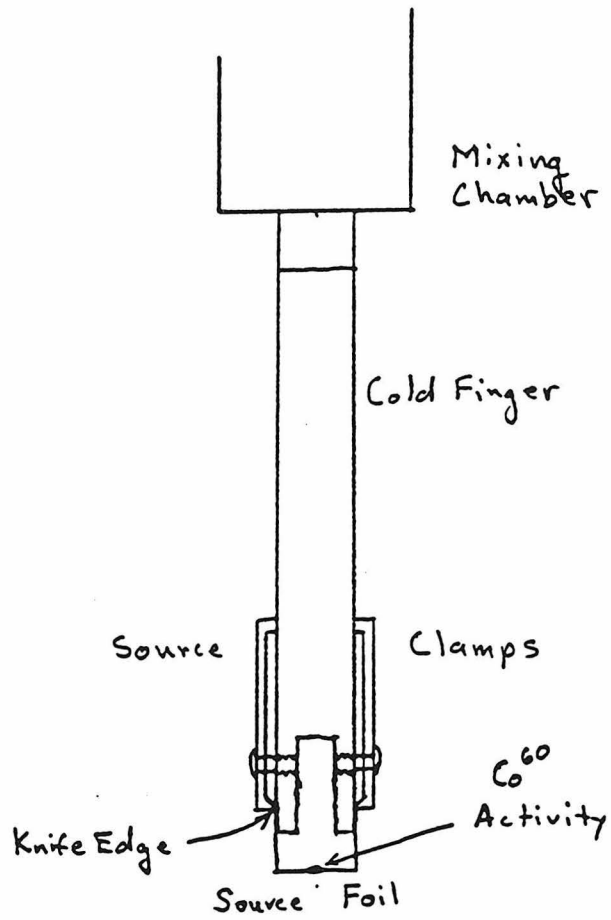


Figure 3.2.6 Source and cold finger geometry

### 3.3 THE POLARIMETER

An electron transverse polarization polarimeter utilizing Mott scattering was designed for this experiment. In order to maximize the polarization analyzing power or sensitivity in a certain counting time, many things have to be considered. The number of electrons scattered from the gold foil relative to the background of gamma rays from the source was of key importance. The scattering asymmetry depends critically on the scattering angle, foil thickness, and the foil geometry. A side view, figure 3.3.1, looking south in the lab along the axis of polarization of the source shows in cross section the geometry of the polarimeter.

Neglecting the effects of multiple scattering in the foil the maximum of the scattering asymmetry for electrons of 150 keV is at 125 degrees as seen in figure 2.3.1 . However, without considering background the analyzing power varies as

$$\text{Analyzing Power} \propto S(\theta) \sqrt{\text{Count Rate}} . \quad (3.3.1)$$

In figure 3.3.2 one can see that this simple argument puts the best scattering angle at about 90 degrees.

The background to measuring the scattered electrons was due to gamma rays from the source. The signal to background is worse for the backward scattering angles because of both the smaller scattering rate and the increase in background as the space available for shielding decreases. The combined effect of these facts led to the choice of 90 degrees for the central scattering angle.

Several geometries of the scattering foil have been used by previous experiments. The two most widely discussed, the transmission and the symmetric designs are shown in figure 3.3.3 along with the reflection geometry. The polarization sensitivity is decreased much more by multiple scattering

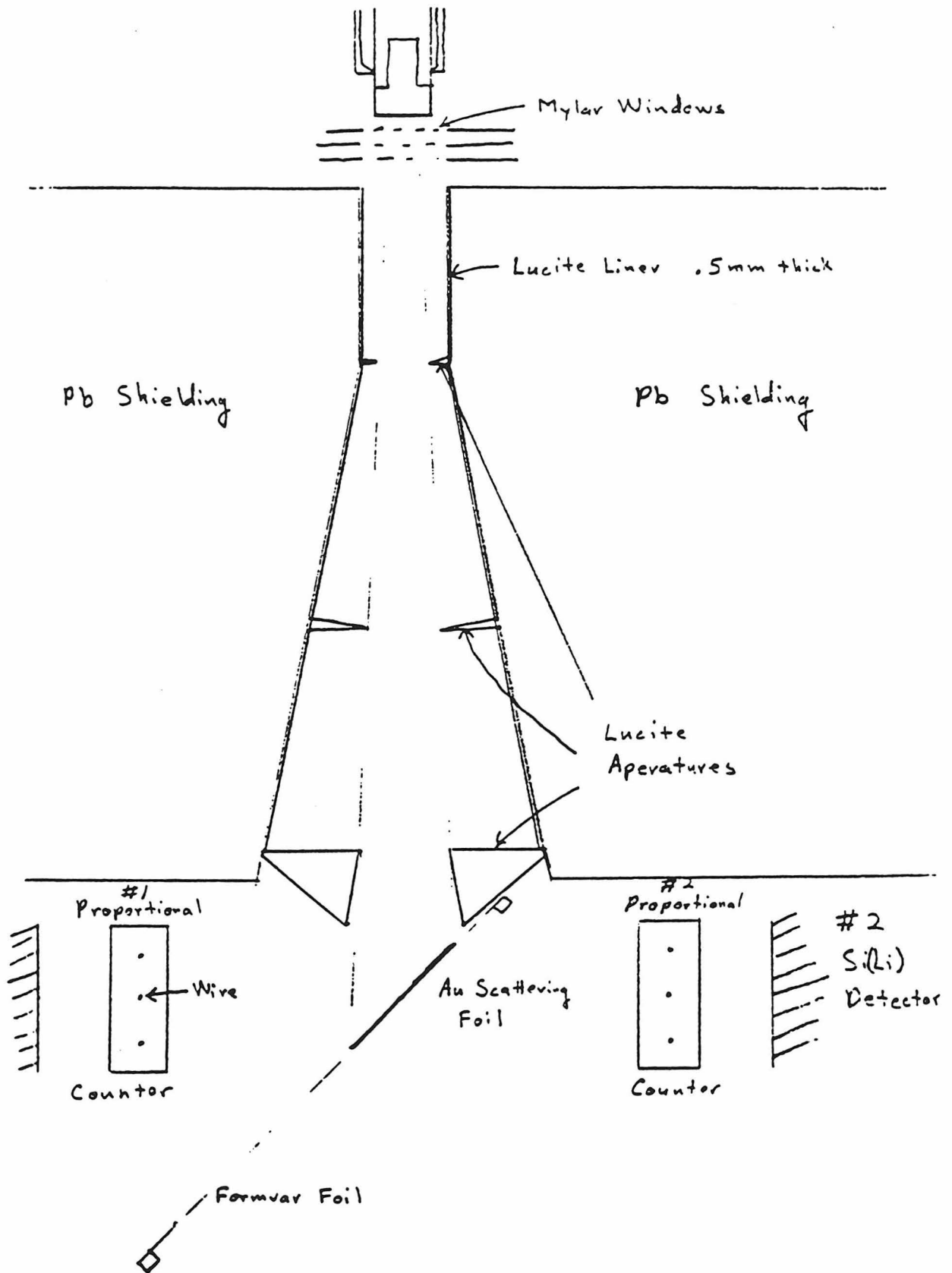


Figure 3.3.1 Polarimeter geometry

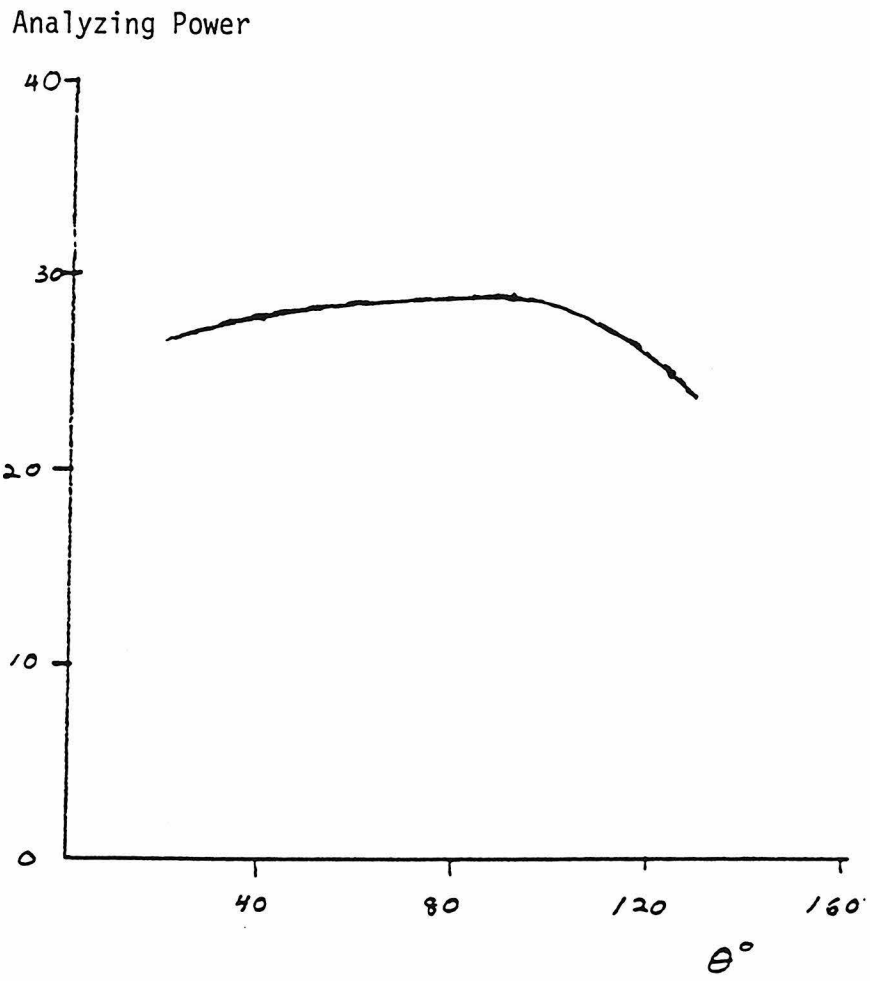
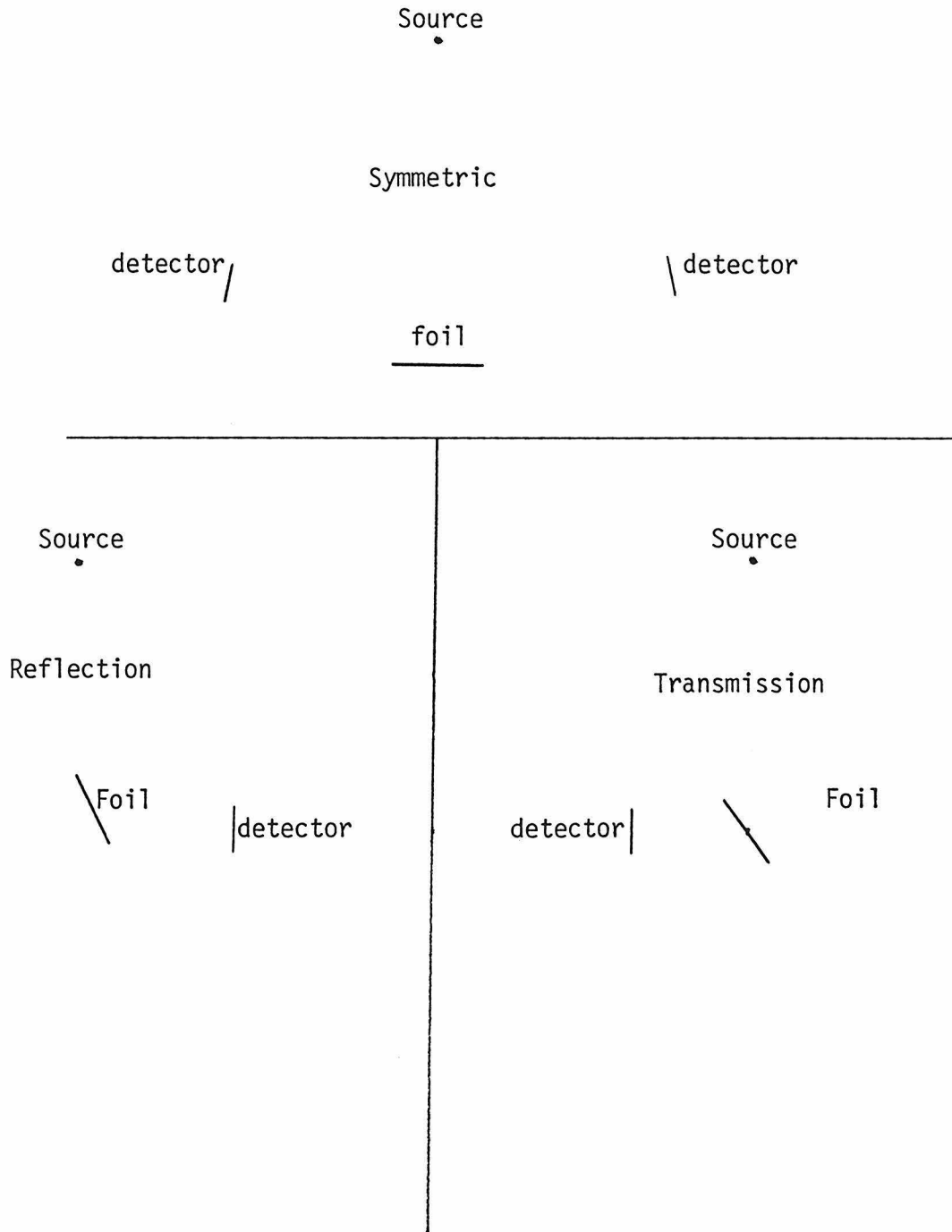


Figure 3.3.2 Zero background analyzing power as a function of angle



in the foil for the symmetric case. For this reason the transmission geometry was chosen for the design.

The choice of the foil thickness is determined by the signal to background and the change in scattering asymmetry with foil thickness. For a wide range of increasing thickness the scattering asymmetry decreases linearly. In this experiment a gold foil of  $135 \text{ micro g / cm}^2$  was used. Multiple scattering decreases the asymmetry by about 15 % at an energy of 150 keV. The gamma background was about equal to the scattered electron rate for this foil at this energy. The analyzing power varies as

$$\text{Analyzing Power} \propto \frac{S(t) \text{ Signal Count}}{\sqrt{\text{Background} + \text{Signal}}}$$

where the thickness is in units of  $135 \text{ micro g / cm}^2$ . One can see that the maximum is near three but it is not a very strong function of  $t$ . A choice of  $t = 1$  was influenced by two considerations. Rather than simply maximizing this analyzing power the effect should be kept as large as possible to minimize sensitivity to systematic effects. In addition this treatment only dealt with 150 keV electrons, for lower energy electrons the maximum analyzing power is at smaller values of  $t$  due to the reduced asymmetry with the increase in multiple scattering as seen in figure 2.3.3.

The gold scattering foil was made by evaporating gold onto a formvar backing. The formvar was first applied to the surface of a glass plate in a similar way as in Revell et al<sup>37</sup>. The gold was evaporated on the formvar while it was still on the glass plate. The formvar and gold were then floated off the glass in a water bath and installed in the foil holder. The thickness of the formvar,  $15 \pm 5 \text{ g / cm}^2$ , and the gold  $135 \pm 10 \text{ g / cm}^2$  were measured by the energy loss of alpha particles from Th-228.

The electronics used in the experiment are shown in the diagram in figure 3.3.5. The Si(Li) detectors have a 2.54 cm diameter with a 5 mm

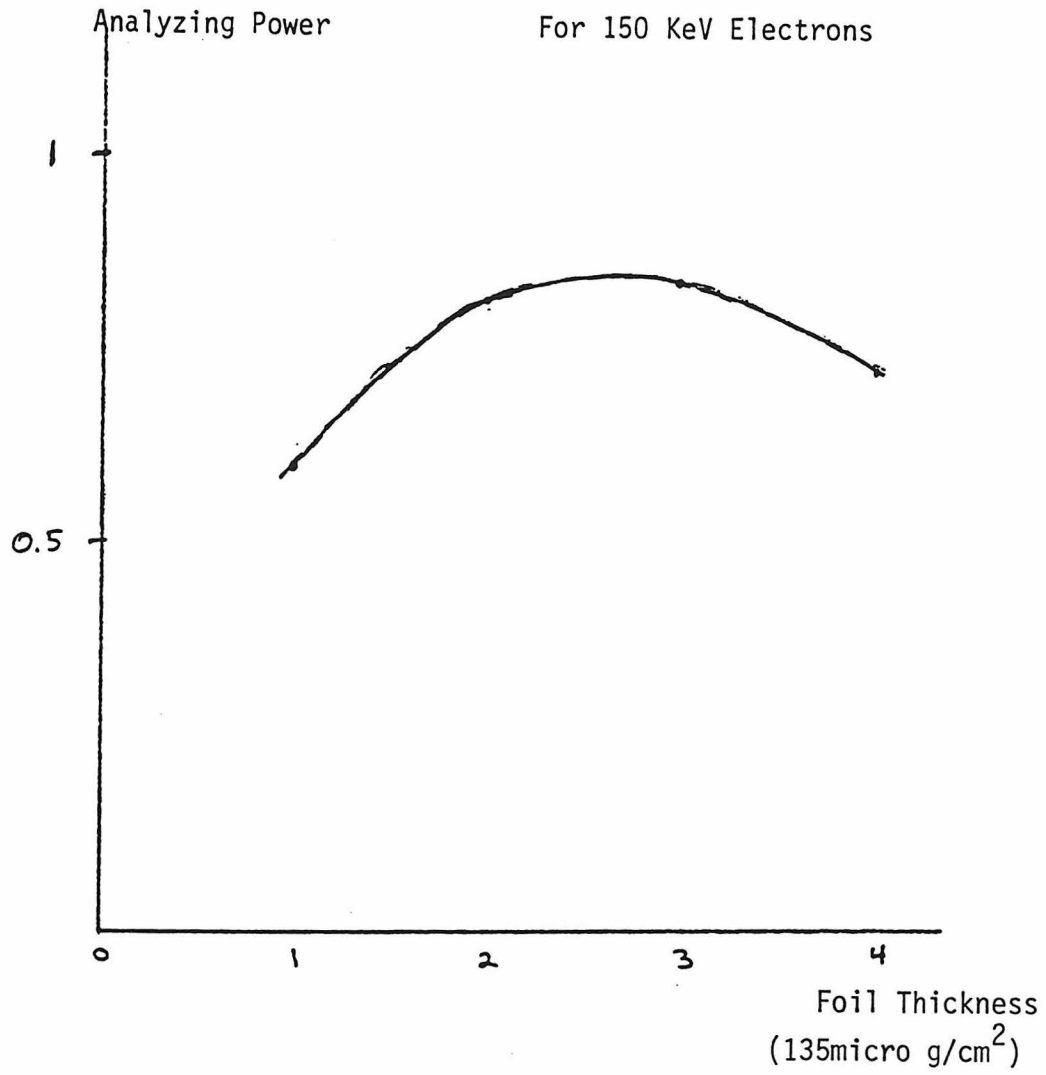


Figure 3.3.4 Analyzing power as a function of foil thickness

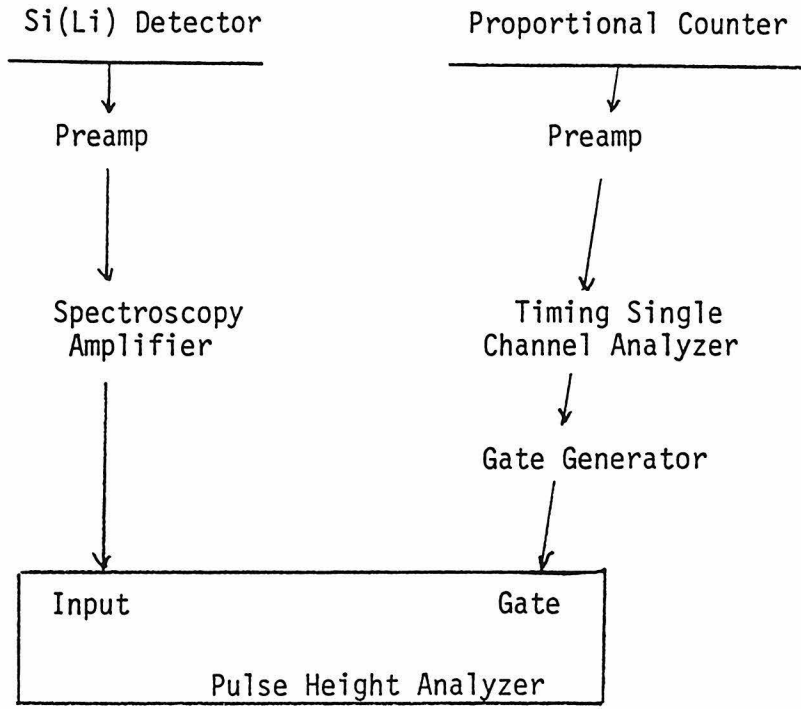


Figure 3.3.5 Electronics Setup

depletion depth. The proportional counters are shown in figure 3.3.6. A mixture of 90 % Argon and 10% methane was used as the counter gas. In order to reduce the gamma ray background the proportional counters and the Si(Li) detectors were used in coincidence. The proportional counter was used to create a gate for the scattered electrons. The timing resolution of the proportional counter and Si(Li) detector systems were about 150 nanoseconds. A gate pulse of 4 micro seconds was used to gate the Si(Li) detector at the pulse height analyzer. Because of the small gamma ray efficiency of the proportional counters the gamma ray background in the Si(Li) detectors was reduced by a factor of 100.

The polarimeter was attached to the outside of the dilution refrigerator room temperature vacuum chamber. The vacuum of the polarimeter was separate from the refrigerator. The source was separated from the polarimeter by three Mylar windows. with a total thickness of 450 micro g /cm.<sup>2</sup>

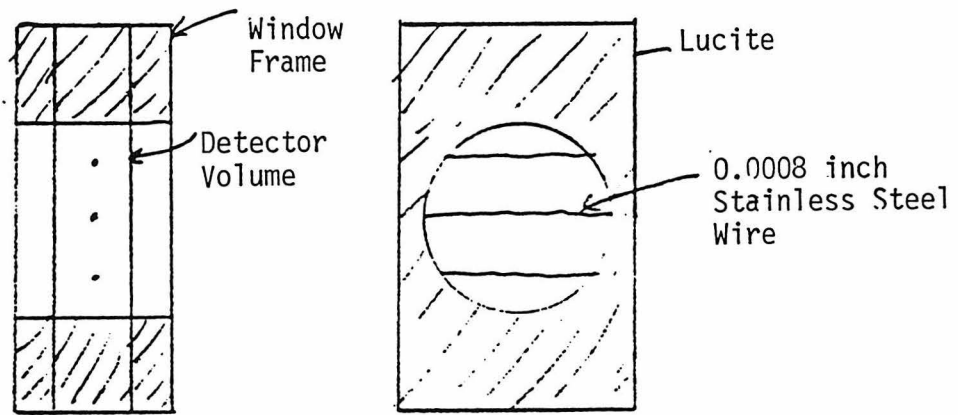


Figure 3.3.6 Proportional counter

### 3.4 THE MEASUREMENT OF NUCLEAR POLARIZATION

The nuclear polarization of the 60-Co source in this experiment was determined from the change in the gamma ray distribution. For both the 1.17 and 1.33 MeV gamma rays the directional distribution is

$$W(\theta) = 1 + \sum B_K U_K A_K Q_K P_K(\cos \theta) = 1 - 0.4164 B_2 P_2(\cos \theta) - 0.2331 B_4 P_4(\cos \theta). \quad (3.4.1)$$

In order to know the nuclear polarization at millikelvin temperatures the gamma ray spectrum in a germanium detector was measured continuously through the experiment. The relative change in the two gamma ray rates at 90 degrees from the axis of polarization between liquid helium and millikelvin temperatures determines the nuclear orientation. One measures

$$\Delta = \frac{W(90) \text{ at } mK}{W(90) \text{ at } 4^\circ} = 1 + 0.208 B_2^{mK} - 0.087 B_4^{mK}. \quad (3.4.2)$$

Using the nuclear magnetic moment of  $+3.81 \pm 0.01$  and assuming all of the nuclei see the saturation hyperfine field of  $-282 \pm 4$  KG the nuclear orientation parameters are uniquely related to delta. In figure 3.4.1 is a plot of the nuclear polarization versus delta.

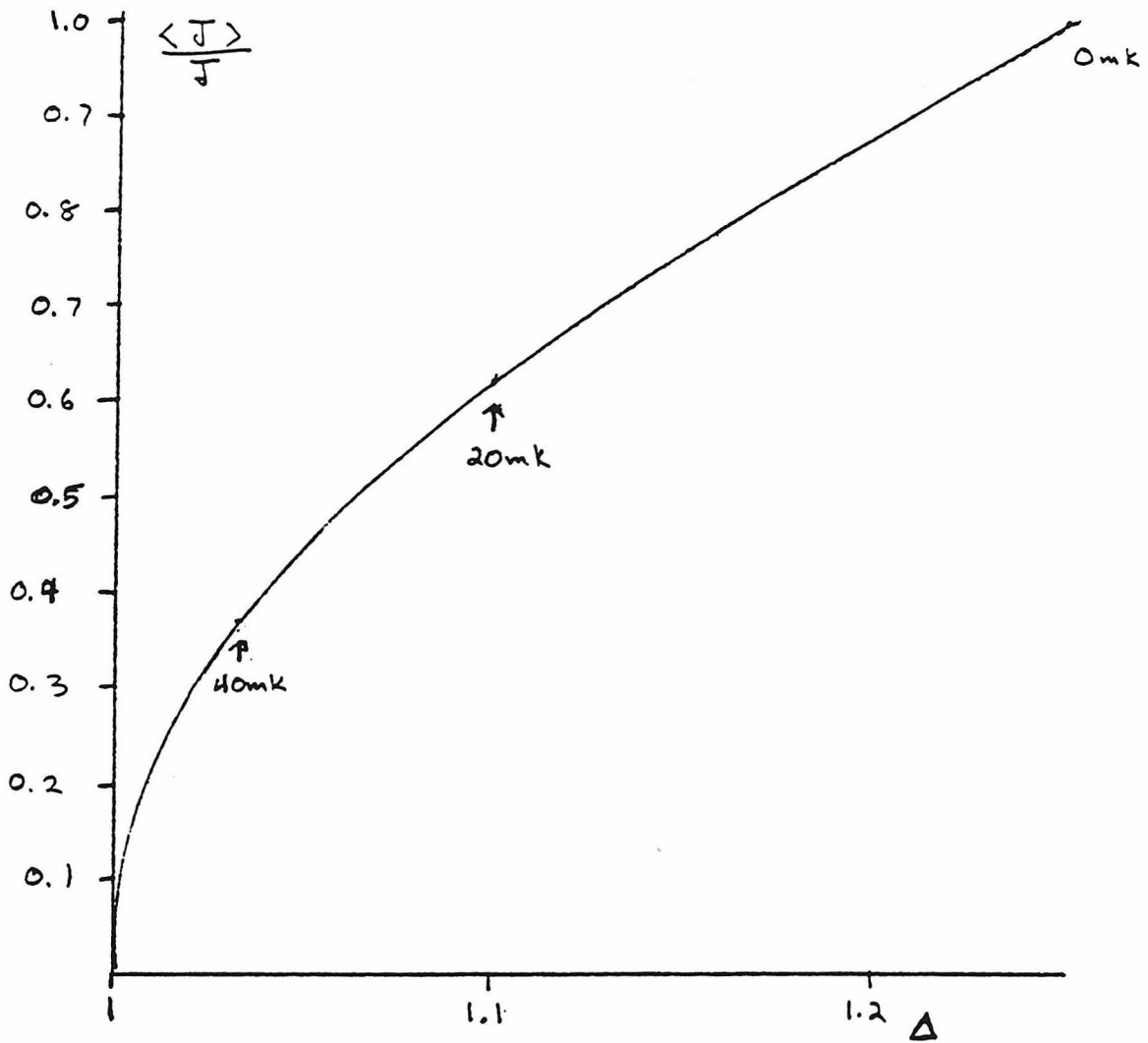


Figure 3.4.1 Nuclear polarization of  $^{60}\text{Co}$  as a function of measured  $\Delta$

### 3.5 MEASURED SCATTERING ASYMMETRIES

The data for this experiment were taken in four separate runs. The polarimeter was aligned as shown in figure 3.5.1. The first two runs were done with the 65 micro Ci source and the next two runs used the 50 micro Ci source both described in section 3.2 . For run 1 the external magnetic field used to saturate the source foil was pointing north and for run 2 the field was reversed . The energy spectra from the Si(Li) detectors gated by the proportional counters were measured for about 10 hour intervals in the pulse height analyzers and recorded. Between each interval the refrigerator was refilled with LN and once a day refilled with LHe. The runs were started by cooling the refrigerator down to the lowest temperature that could be achieved of about 35mK. Data were taken for several intervals at millikelvin temperatures then the refrigerator was warmed to LHe temperature for data taking for several more intervals.

The gamma ray energy spectrum of a germanium detector positioned perpendicular to the axis of nuclear polarization of the source was continuously measured in order to know the nuclear polarization. Table 3.5.1 gives the average nuclear polarization of the 60-Co nuclei during the intervals at millikelvin temperatures for the four data runs. A lower temperature and thus greater nuclear polarization was achieved for runs 3 and 4 with the weaker 50 micro Ci source. This is expected because for these sources the temperature obtainable was limited by the selfheating generated by the nuclear decay energy deposited in the source foil.

The cumulative proportional counter gated spectra from the Si(Li) detectors for the intervals of run 1 with the source at LHe temperature are shown in figure 3.5.2. The background spectra due to the gamma rays from the source were very nearly identical in the two detectors. They were

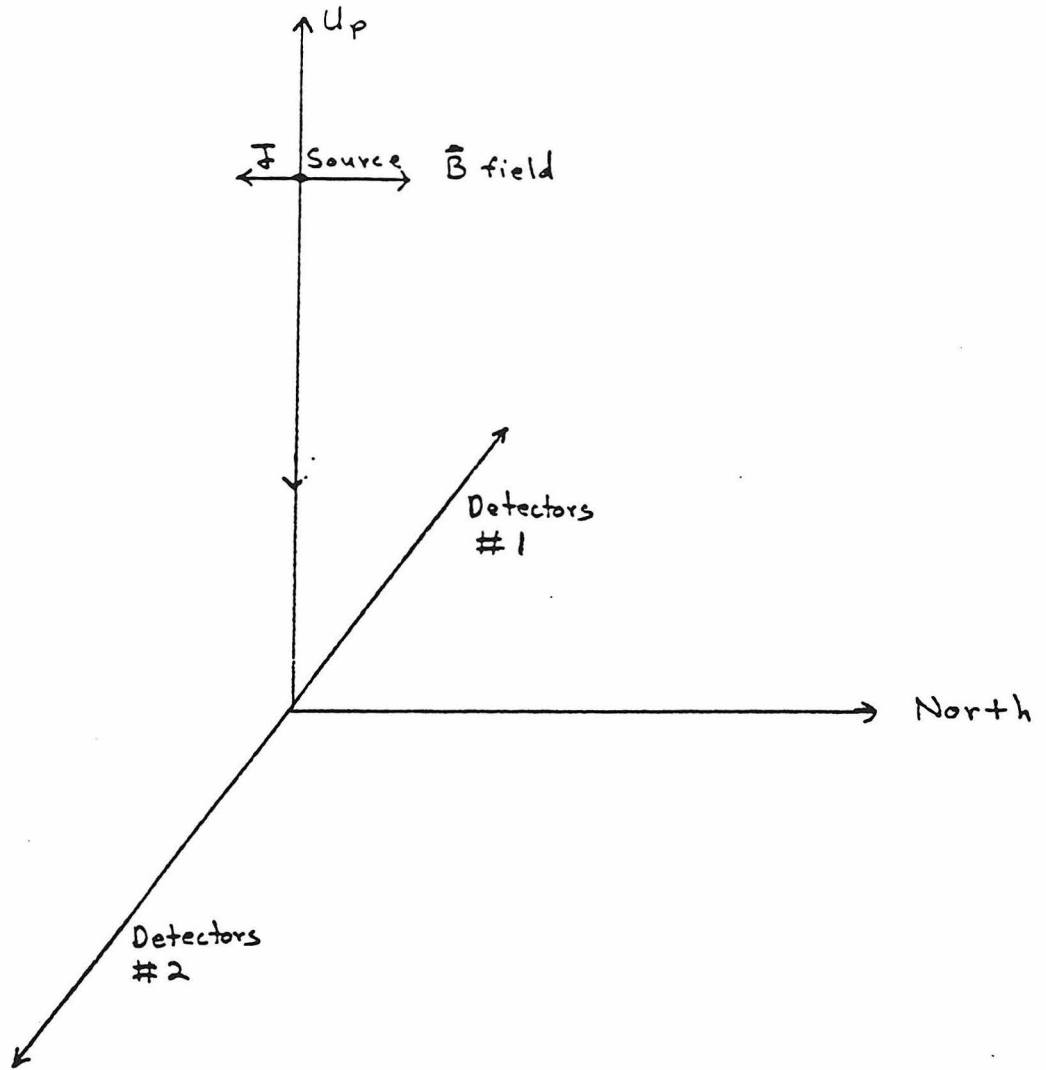


Figure 3.5.1 Geometry of source, field and detectors

RUN	SOURCE STRENGTH	$\langle J \rangle / J$
1	65 micro Ci	0.41± 0.01
2	65 micro Ci	0.39± 0.01
3	50 micro Ci	0.43± 0.01
4	50 micro Ci	0.45± 0.01

Table 3.5.1 Nuclear polarization

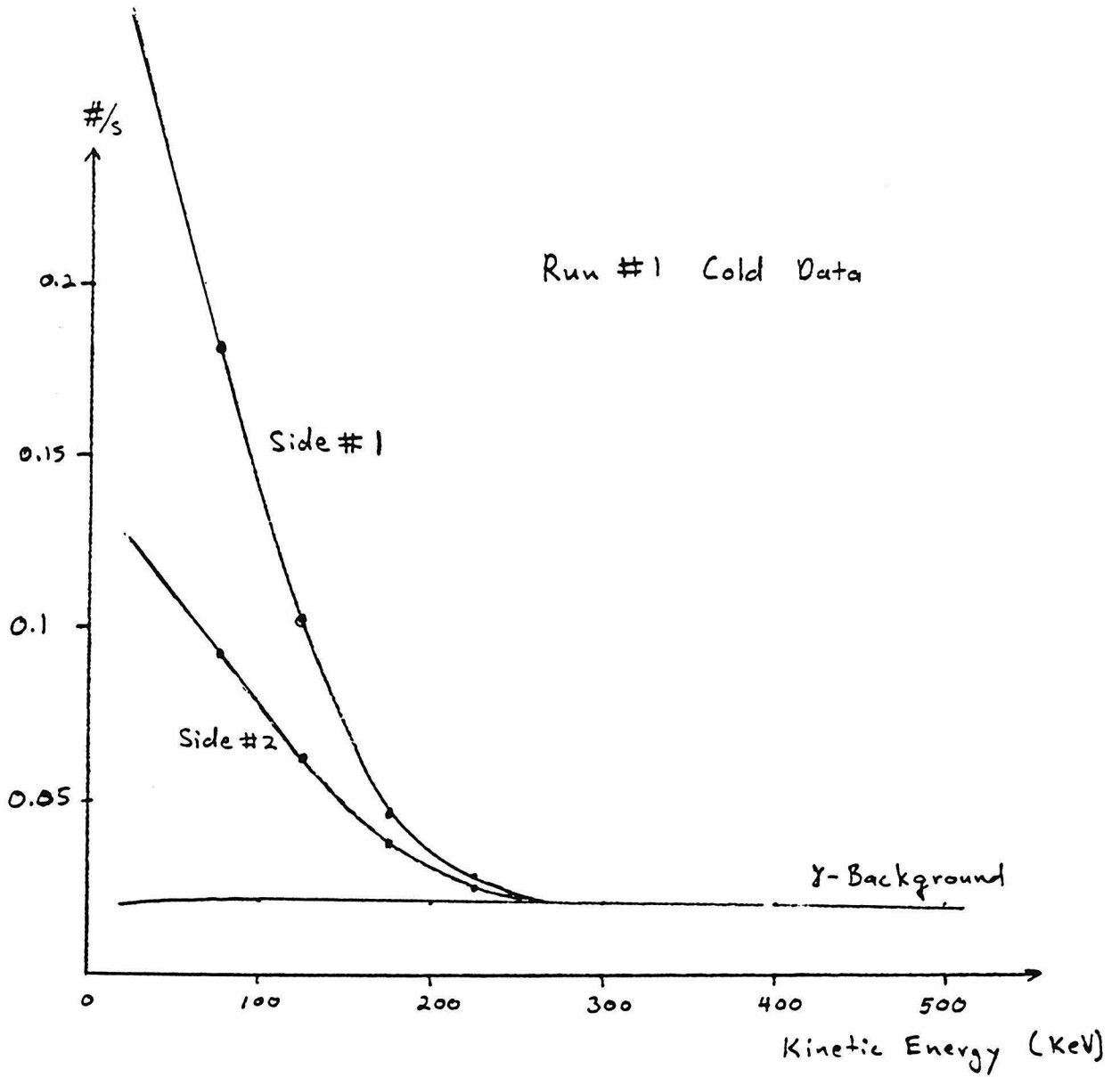


Figure 3.5.2 Run #1 cold data gated spectra

measured at room temperature by replacing the scattering foil with a formvar foil of the same thickness used as the backing for the gold scattering foil.

From the measured spectra the asymmetries,

$$A_i^{\text{cold}}(E, \Delta E) = \frac{N_1 - N_2}{N_1 + N_2} \frac{T}{T_i} \text{ warm} \quad , \quad A_i^{\text{warm}}(E, \Delta E) = \frac{N_1 - N_2}{N_1 + N_2}$$

can be calculated for the i-th measuring interval from an energy interval centered at E, E wide, where N is the number of counts within this energy range from Si(Li) detector 1 and N is from detector 2. Cold, Warm refers to the temperature of the source being at millikelvin or LHe temperature respectively. To eliminate polarization dependent effects from the denominator of the asymmetries and thus simplify the analysis, LHe temperature counts are used to normalize the asymmetries. The  $A_i$  are normalized by the total LHe count in the energy interval for this run. A correction for the different counting times of each interval is accomplished by the factor T (the total LHe counting time) /  $T_i$  (the i-th interval time). In figure 3.5.3 the asymmetries from many energy intervals for the measuring intervals of run 1 are plotted. Figure 3.5.4 has the results from run 2 for which the field was reversed. Two runs were taken with the second source of 50 micro Ci and the asymmetries are shown in figures 3.5.5 and 3.5.6 .

During all of the runs there was no significant drift in the data with time. Thus, in the forthcoming analysis for each run the data from the intervals when the source was cold, millikelvin, will be added together and likewise for the LHe data intervals.

For each run the difference ,

$$\Delta A(E, \Delta E) = \frac{(N_1 - N_2)^{\text{cold}}}{(N_1 + N_2)^{\text{warm}}} - \frac{(N_1 - N_2)^{\text{warm}}}{(N_1 + N_2)^{\text{warm}}}$$

between the counting asymmetry measured with polarized 60-Co at millikelvin temperature and the asymmetry measured with unpolarized 60-Co at

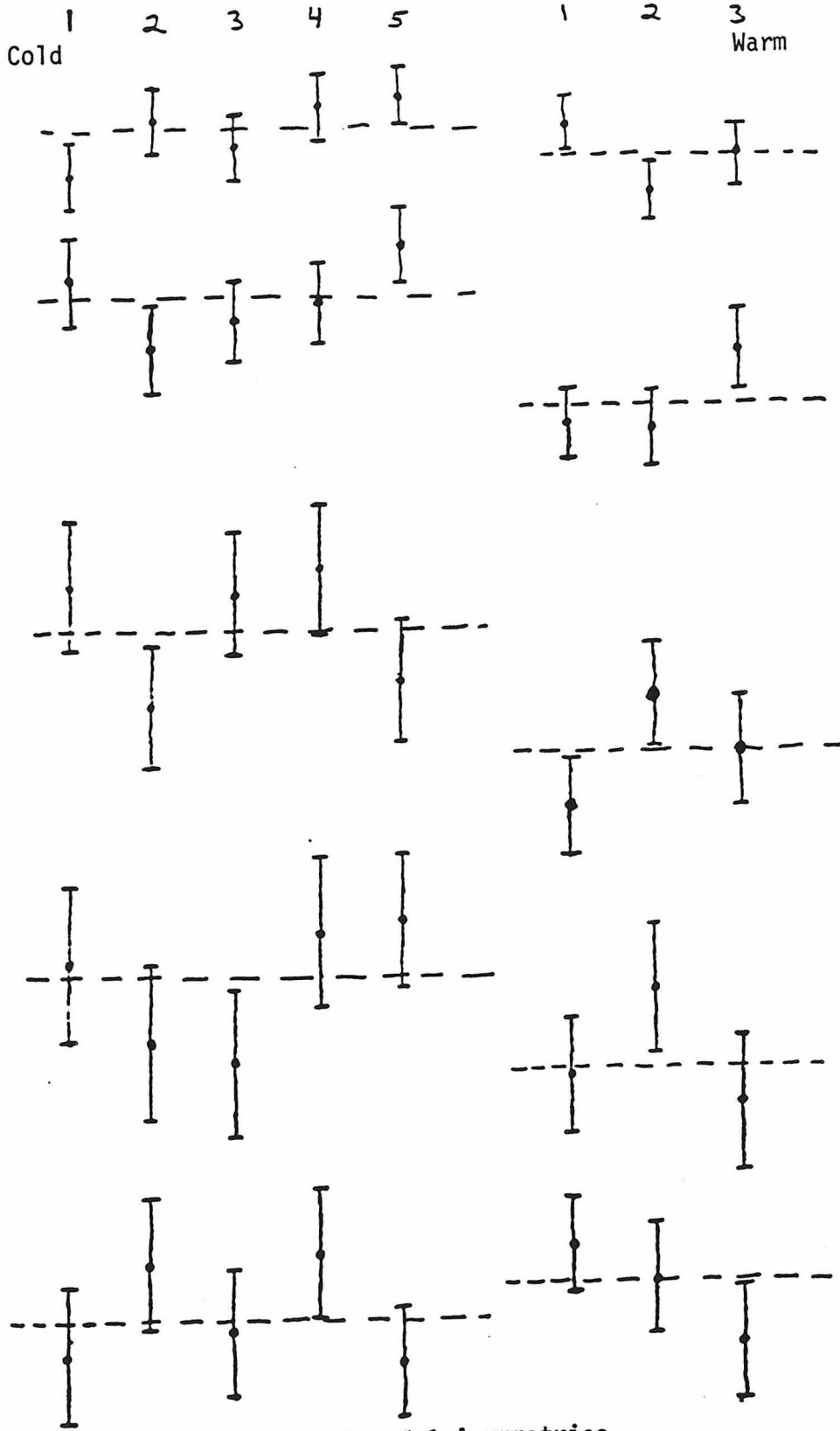


Figure 3.5.3 Run # 1 Asymmetries

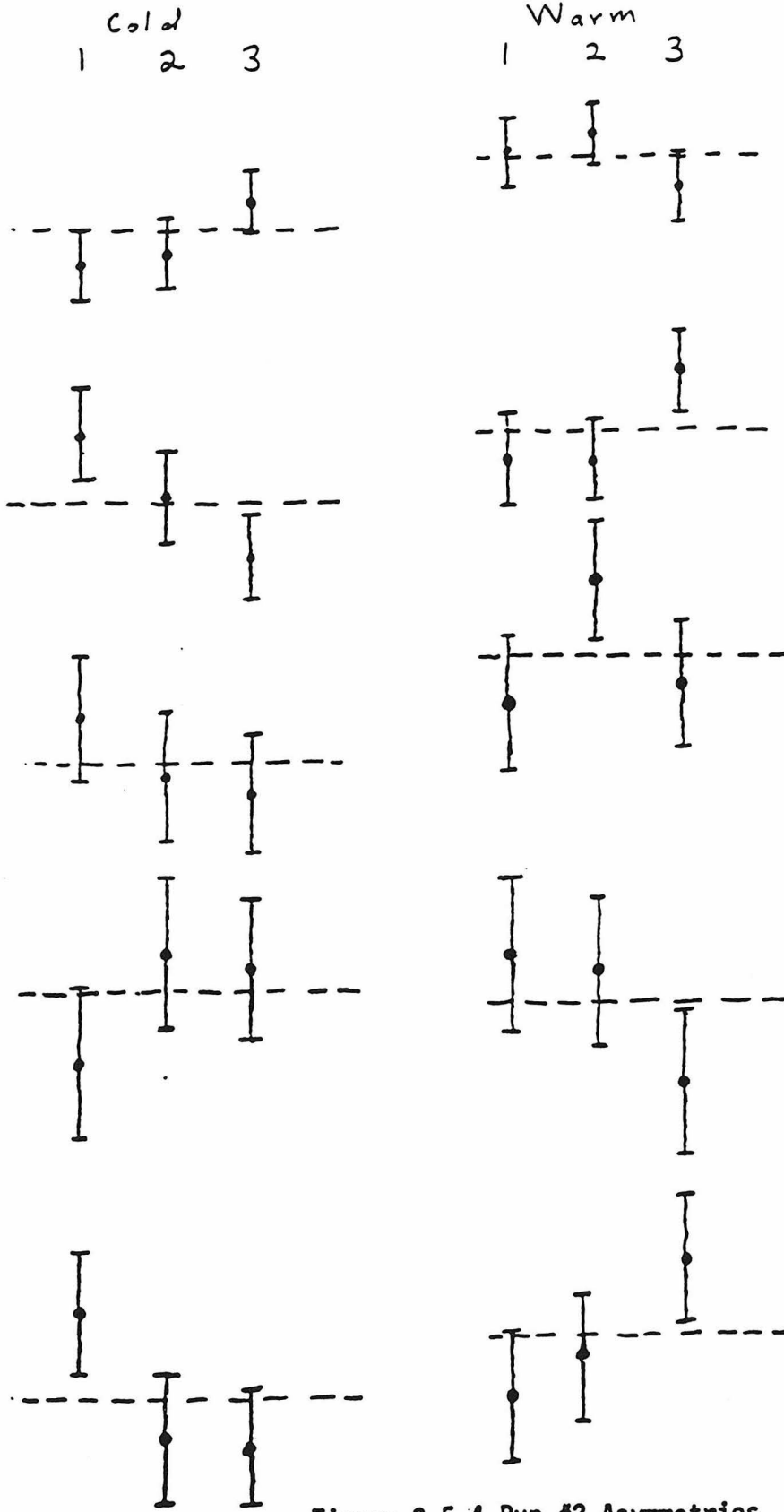


Figure 3.5.4 Run #2 Asymmetries

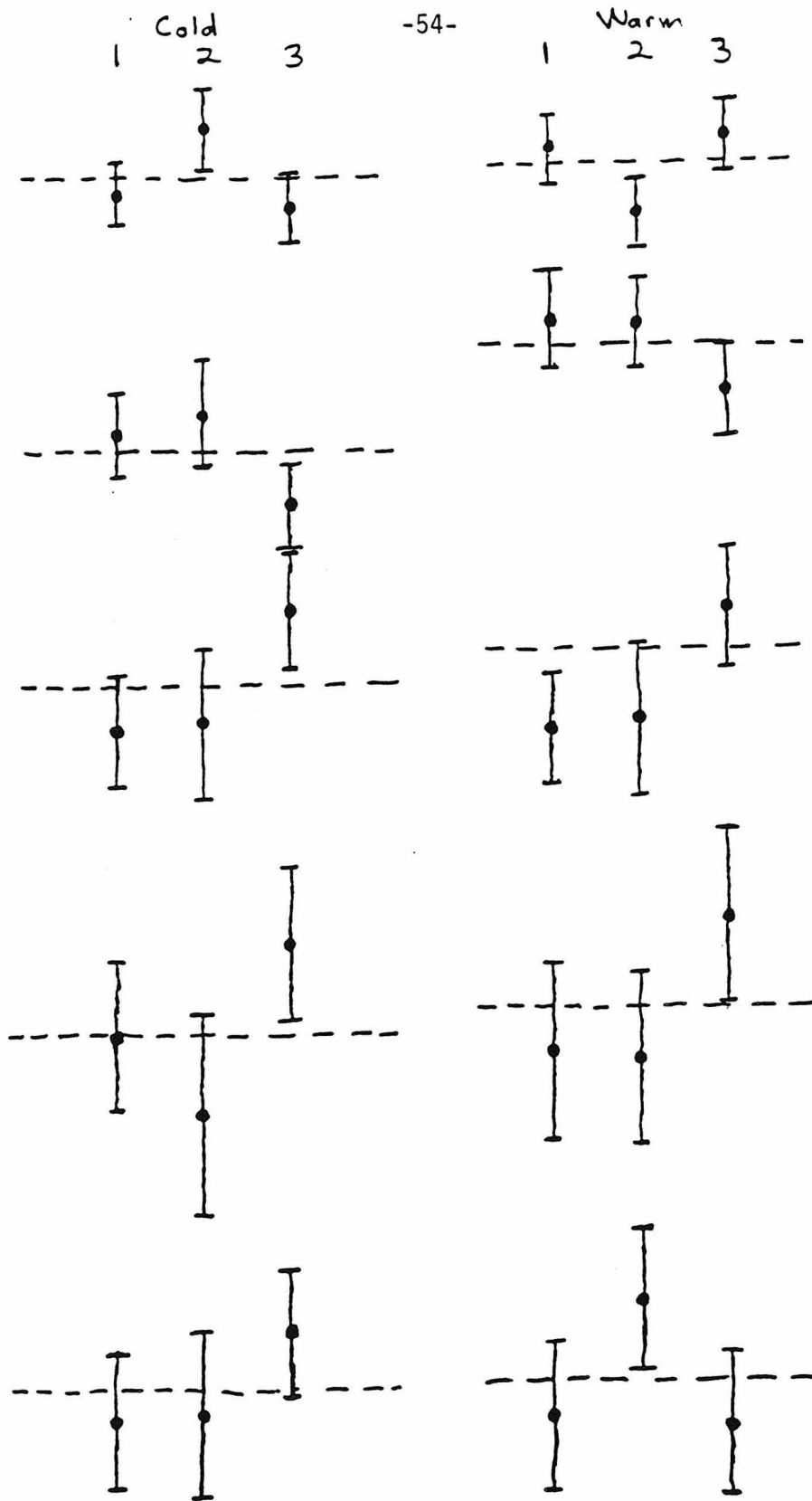


Figure 3.5.5 Run #3 Asymmetries

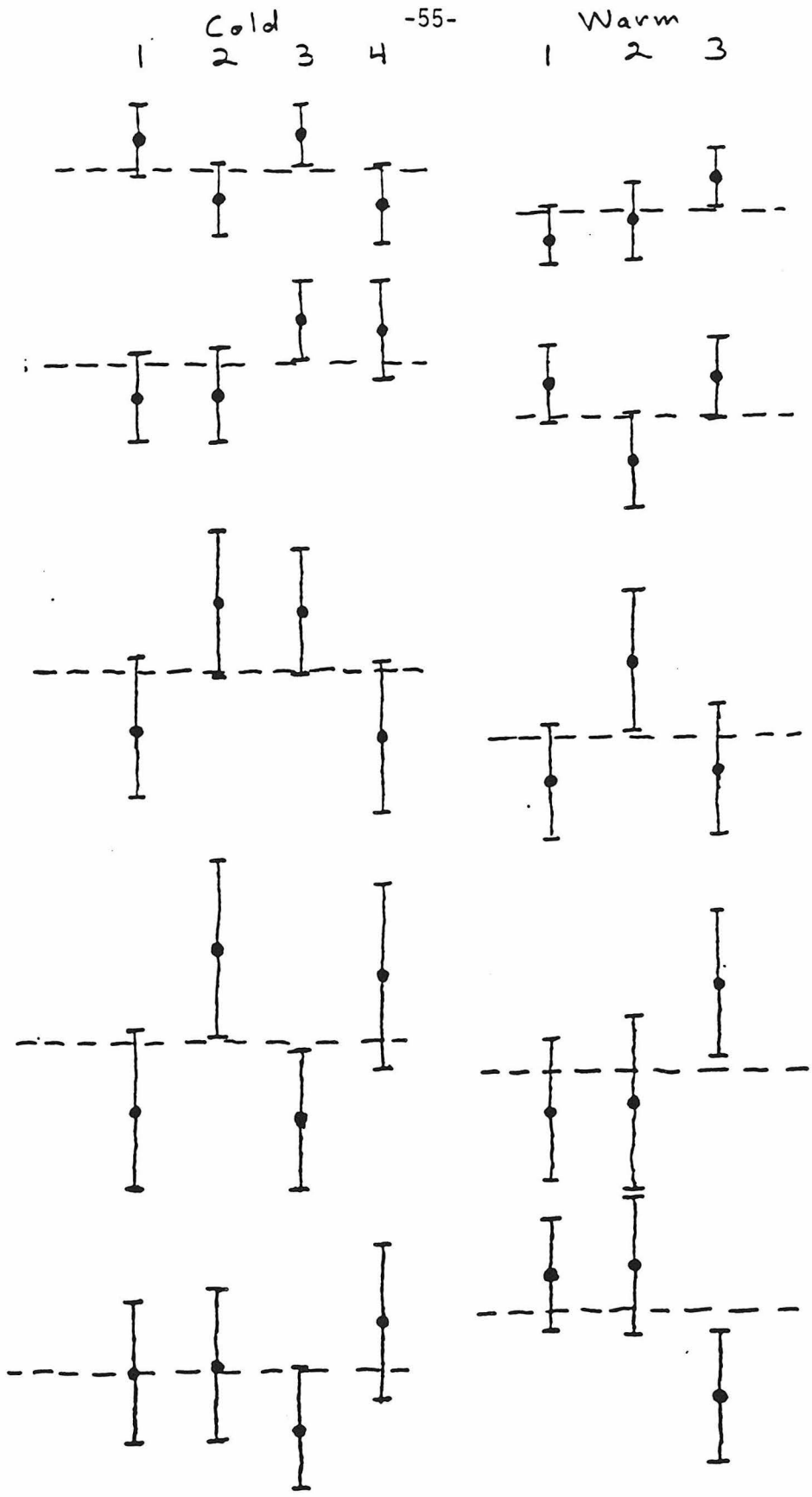


Figure 3.5.6 Run #4 Asymmetries

The temperature is a measurement of the transverse polarization of the beta particles that enter the polarimeter from the polarized  $^{60}\text{Co}$ . Figure 3.5.7 shows  $A(E, \Delta E)$  for the four runs completed. In the next section this experimental result will be compared to the expected effect based on the theory of the transverse polarization of beta particles from the decay of polarized nuclei and the known polarization sensitivity of the Mott scattering of electrons from gold foils.

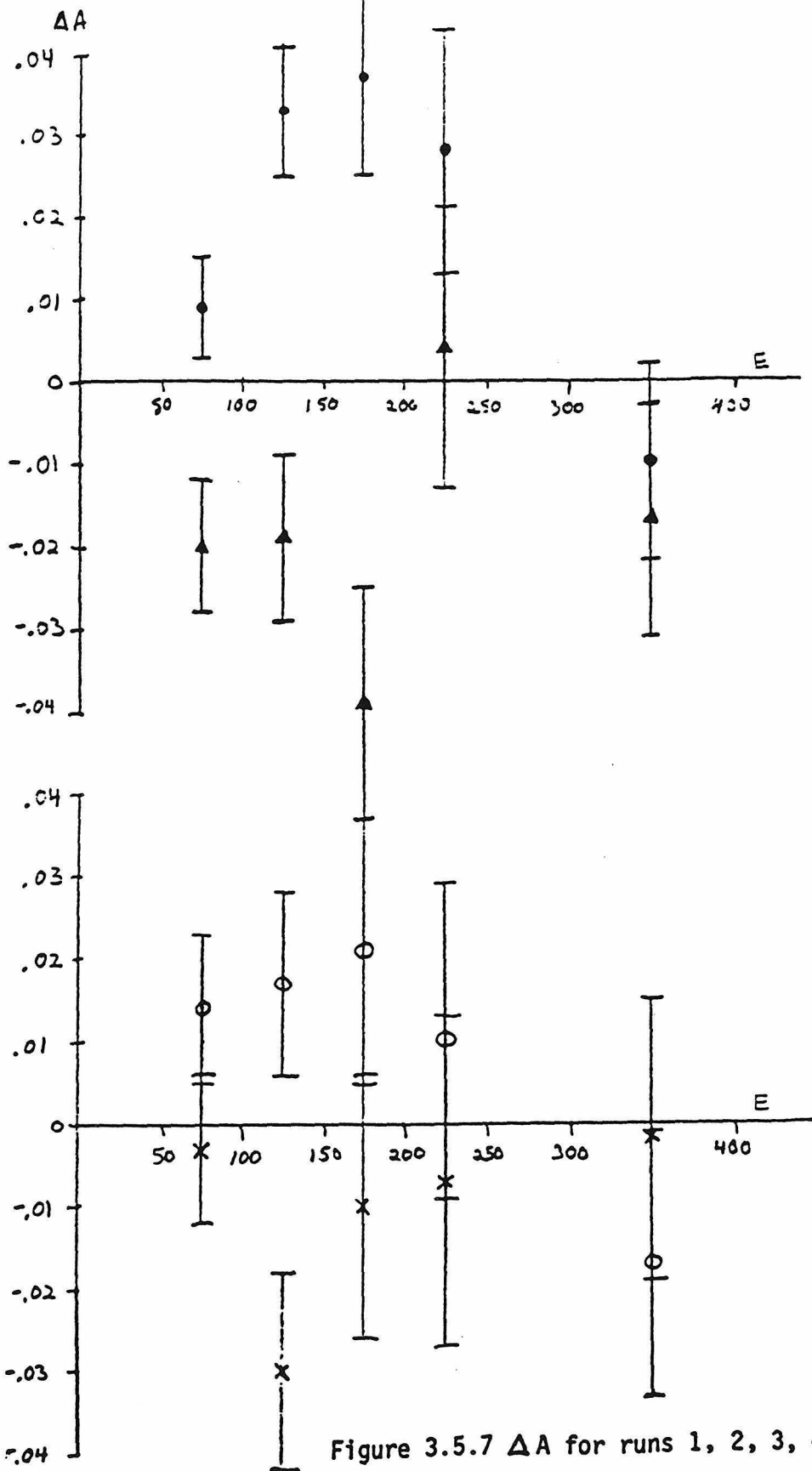


Figure 3.5.7  $\Delta A$  for runs 1, 2, 3, 4

### 3.6 BETA PARTICLE SPECTRUM AND PREDICTED POLARIZATION

In order to compare the measured scattering asymmetry change  $A(E, \Delta E)$ , described above to the predicted effect based on the theory of the polarization of beta particles from the decay of oriented nuclei and the polarization sensitivity of Mott scattering, several things must be included. The predicted transverse polarization and the energy spectrum of the electrons as they enter the polarimeter must be known. With these as input the change in asymmetries for the measured spectra can be calculated using the expected Mott scattering cross sections from theoretical calculations and previous experimenter's results. The goal is to determine whether the experimental results presented in section 3.5 are in agreement with the predictions of beta decay theory. The energy spectrum of beta particles that enter the polarimeter is determined in this section. The polarization of electrons is calculated based on the purely V - A weak interaction result for the distribution in momentum and polarization for electrons from the decay of polarized  $^{60}\text{Co}$ .

The beta energy spectrum shown in figure 3.6.1 is from a  $^{60}\text{Co}$  source prepared as in section 3.2 . It was measured using one of the Si(Li) detectors of the polarimeter. For this spectrum mylar windows of the same thickness as in the refrigerator were placed over the source. In order to find the actual spectrum of beta particles entering the polarimeter the spectral response of the Si(Li) detector to monoenergetic electrons must be determined. The response function of the detector was measured using a  $^{139}\text{Ce}$  conversion electron source. The measured  $^{139}\text{Ce}$  spectrum and its decay scheme are shown in figure 3.6.2. The variation of the response function with energy is needed to determine the actual spectra of the  $^{60}\text{Co}$  sources. It is assumed that the height of the low energy tail relative to the peak

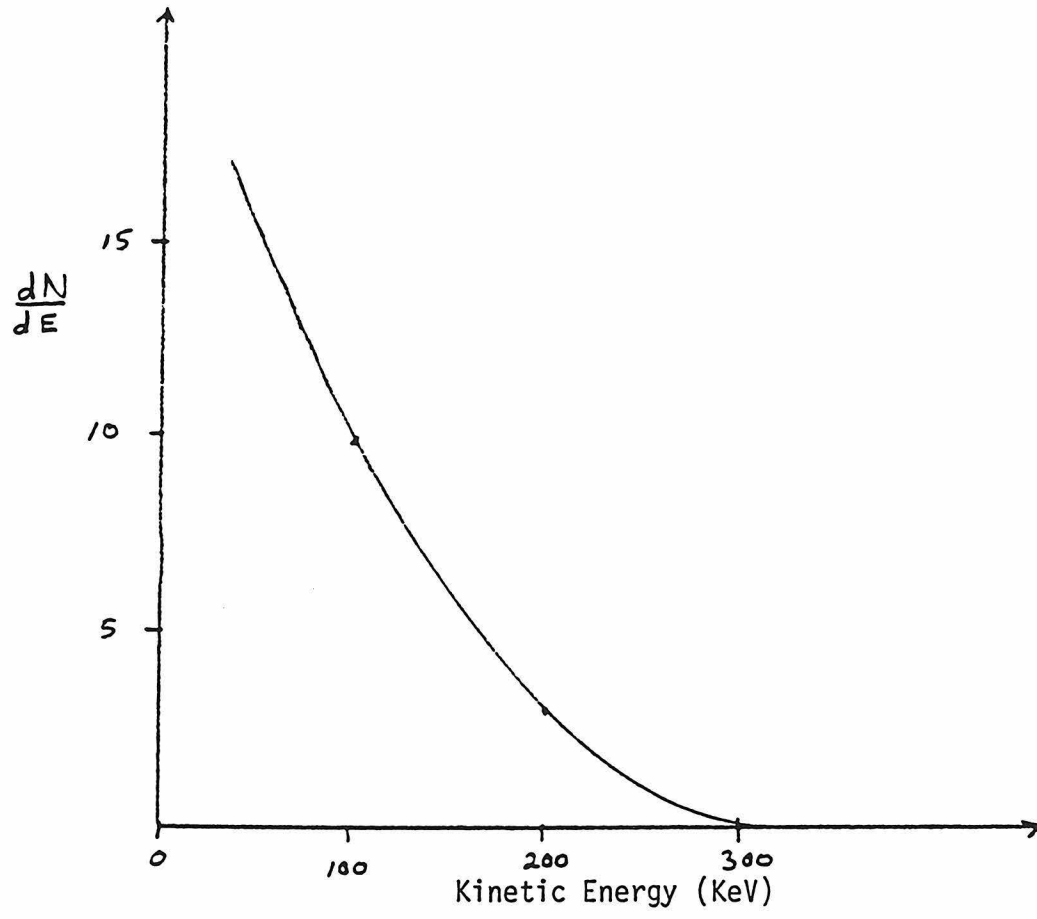


Figure 3.6.1 Beta spectrum from  $^{60}\text{Co}$  source

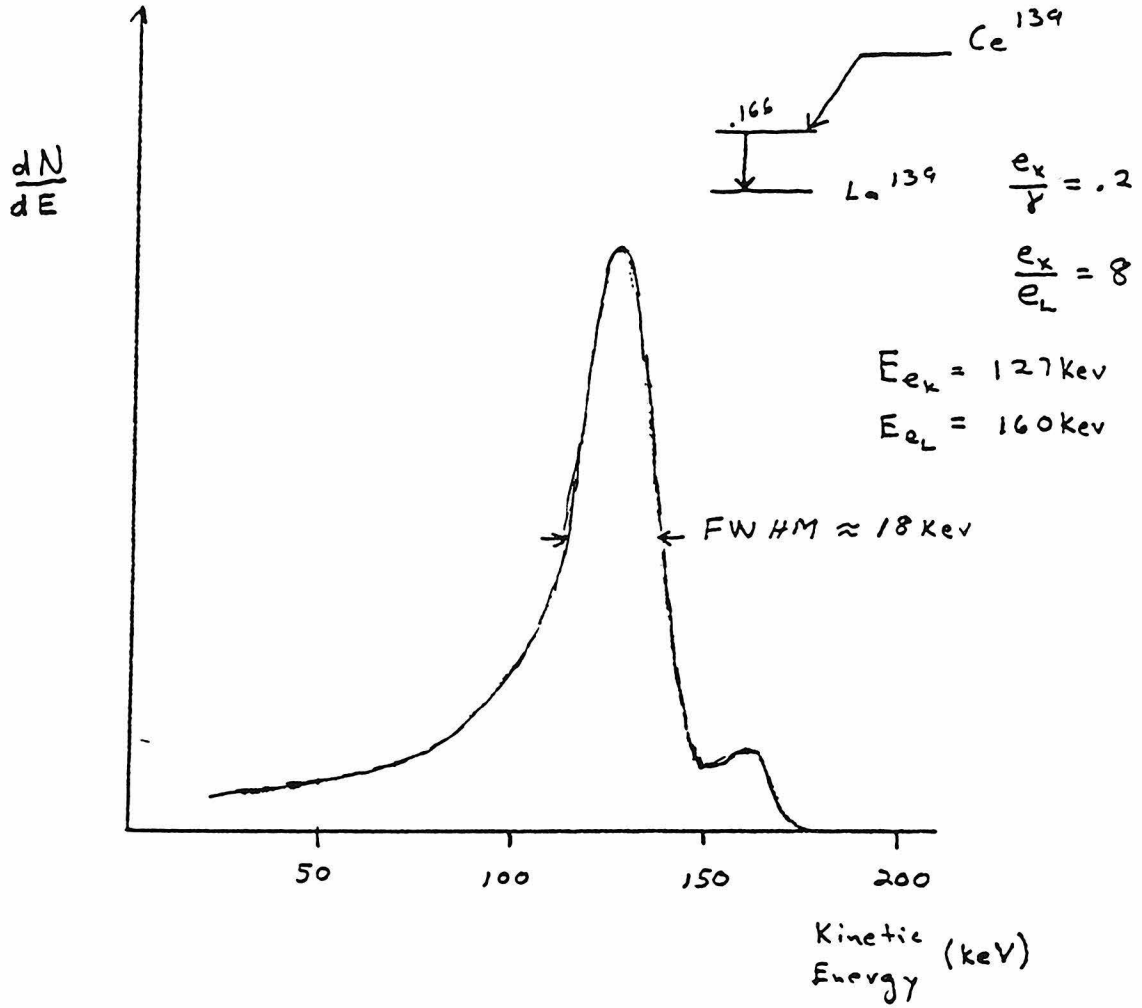


Figure 3.6.2 Si(Li) detector response and  $^{139}Ce$  decay scheme

height increases as the inverse of the kinetic energy of the peak toward low energy. This is used since the tail is due to backscattering from the detector. The width of the energy peak is taken to be constant with energy because it is dominated by the detector noise. Using this response function the spectrum of beta particles entering the polarimeter is calculated and presented in figure 3.6.3 .

The angular distribution of electrons from the decay of polarized 60-Co is

$$W \propto 1 - \frac{v}{c} \hat{p} \cdot \frac{\langle \vec{J} \rangle}{J} \quad (3.6.1)$$

$\hat{p}$  is the direction of the momentum. Figure 3.6.4 shows the relationship between the nuclear polarization, the initial electron momentum direction, and the magnetic field used to saturate the source foil. In the calculation of the expected  $\Delta A$ , the asymmetry for electrons from polarized 60-Co must include the asymmetric distribution of electrons and the deflection of the electron momentum in the magnetic field used to saturate the source foil. For each element of solid angle  $d\Omega_1$  shown in figure 3.6.4 the proper weighting from the distribution equation 3.6.1 is calculated correcting for the magnetic deflection in the y direction.  $B(z)$  is assumed to be only in the x direction. Figure 3.6.5 gives the measured  $B(z)$ . The deflection is determined by

$$\Delta y = \frac{e c}{E v} \int_0^z \int_0^{z'} B(z'') dz'' dz'$$

Here,  $e$  is the electron charge and  $E$  is its total energy. Thus, the solid angle elements get the weighting for undeflected electrons  $\Delta y$  away.

The starting point for determining the predicted transverse polarization of the beta particles that enter the polarimeter is the distribution of beta particles from polarized 60-Co,

$$W \propto 1 - \frac{v}{c} \hat{p} \cdot \frac{\langle \vec{J} \rangle}{J} - \frac{v}{c} \vec{\sigma} \cdot \hat{p} + \frac{\gamma m}{E} \vec{\sigma} \cdot \frac{\langle \vec{J} \rangle}{J} + \frac{E - \gamma m}{E - m} \frac{p}{E + m} \frac{v}{c} \vec{\sigma} \cdot \hat{p} \hat{p} \cdot \frac{\langle \vec{J} \rangle}{J} + \frac{Zm}{E} \frac{\langle \vec{J} \rangle}{J} \times \hat{p} \cdot \vec{\sigma} \quad (3.6.2)$$

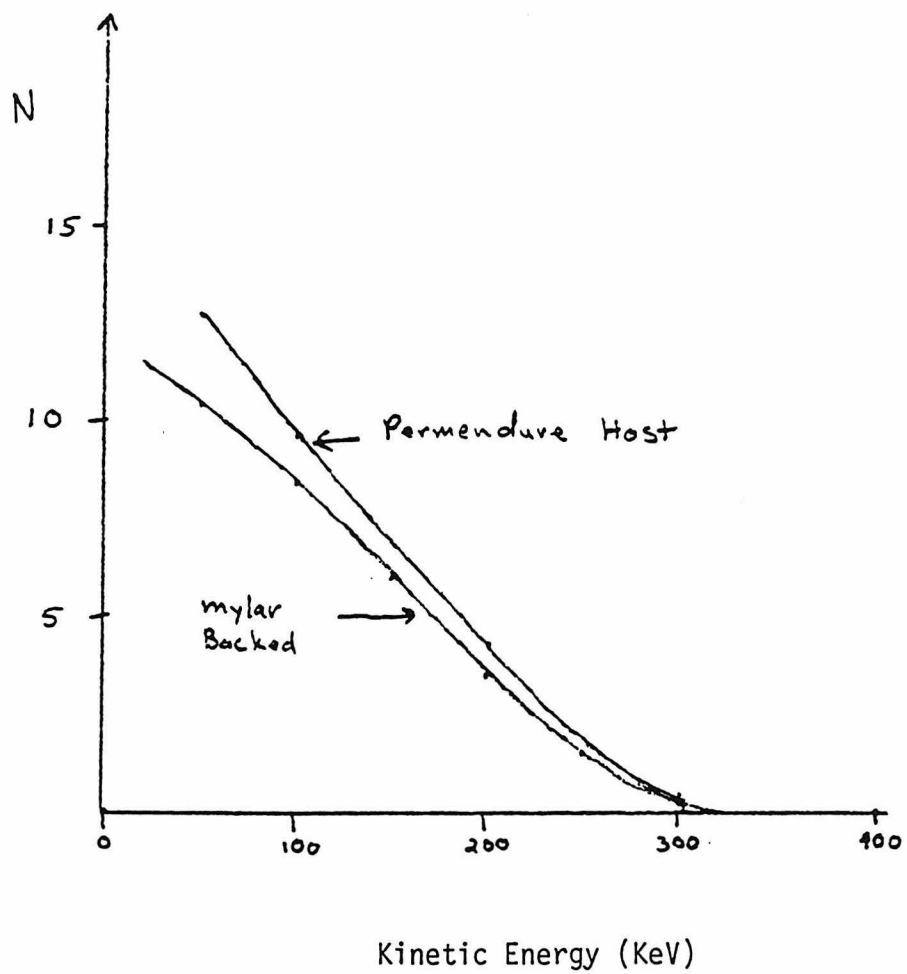


Figure 3.6.3 Response corrected beta spectra

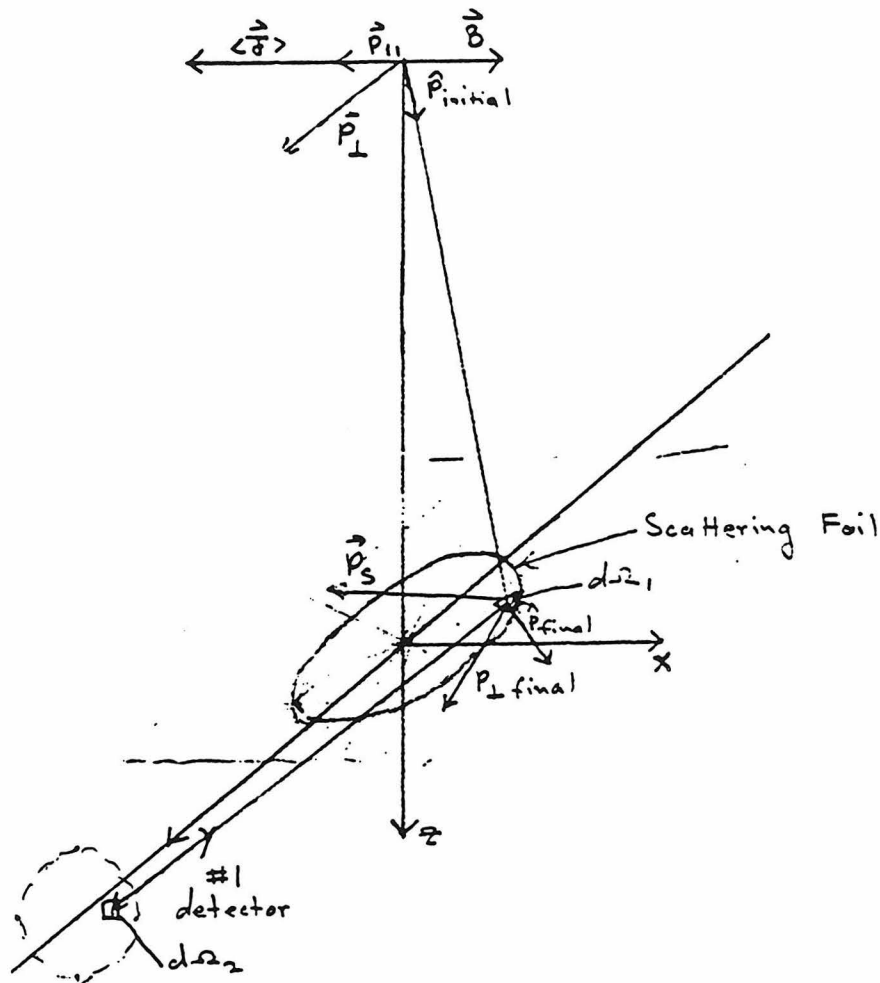


Figure 3.6.4 Scattering geometry and magnetic field trajectories

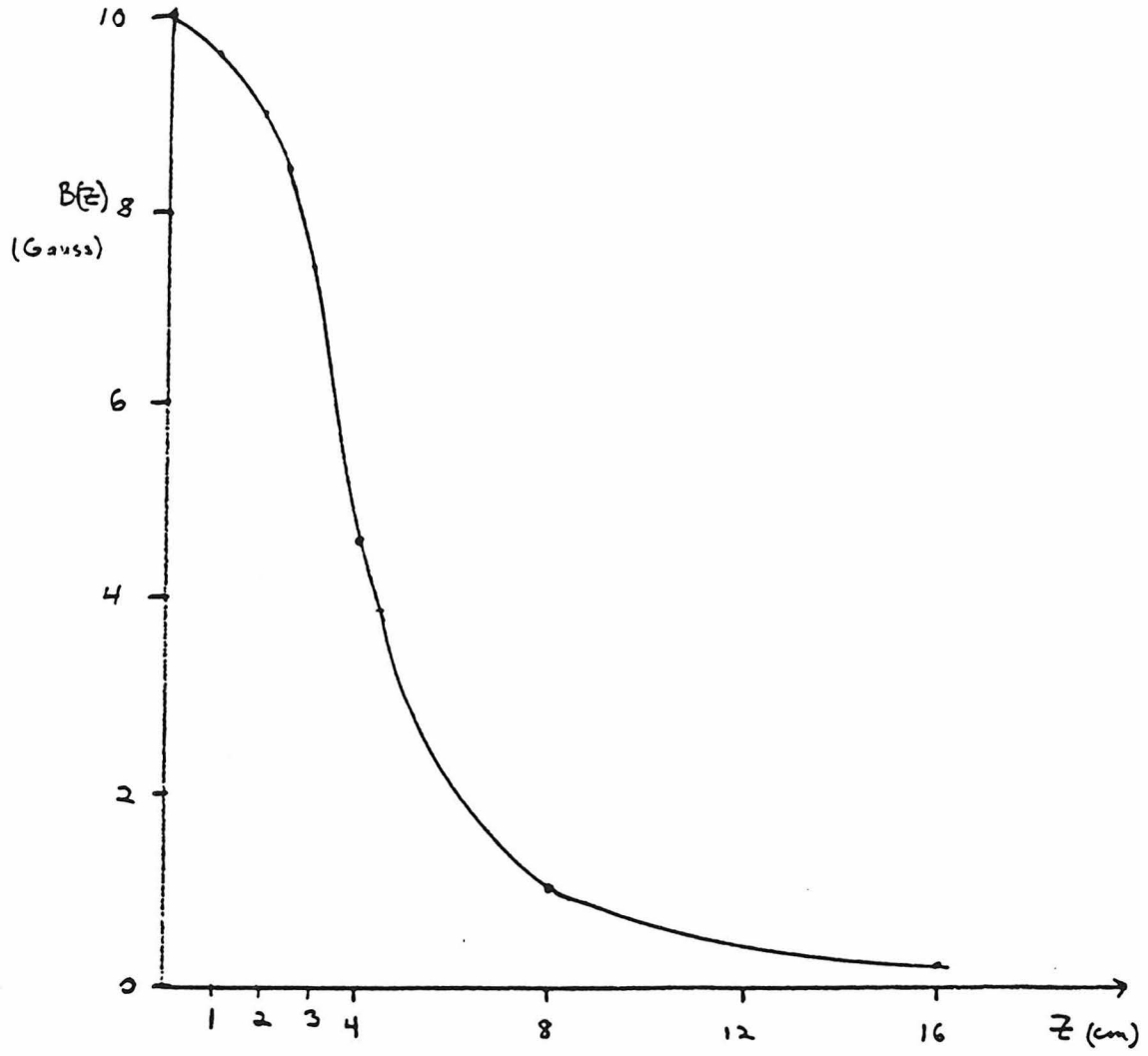


Figure 3.6.5 Measured stray magnetic field distribution

From this distribution the electron polarization for electrons entering the polarimeter is calculated. This predicted transverse polarization must be corrected for the effects of scattering in the source foil and windows of the refrigerator. In addition the effects of the applied magnetic field used to saturate the source foil must be included.

In this analysis the depolarization of the electrons which enter the polarimeter due to scattering in the windows of the refrigerator will be ignored. Using the scattering theory as applied by Scott<sup>38</sup> there are very few expected scatterings in the total Mylar thickness of  $450 \text{ micro g / cm}^2$  at any energy of interest. In addition, because of the low Z of the constituents of Mylar any scattering would not be expected to affect the polarization.

The determination of the reduction of the electron polarization due to the scattering in the source foil was separated into two parts. First, using the measured depth of diffusion of the  $^{60}\text{Co}$  into the surface of the source foil the average depolarization as they exit the foil of beta particles emitted from the nuclei in the direction of the polarimeter can be estimated. Since the expected scattering again based on the theory of Scott is small this contribution to the average depolarization is assumed to be zero.

The transverse polarization of the beta particles entering the polarimeter may be reduced in another way. Many of the electrons which finally enter the polarimeter were initially emitted from the polarized nuclei in other directions. They scatter in the foil and eventually leave the foil surface into the polarimeter. The net result can be a reduction in the average polarization of the the electrons reaching the polarimeter. In figure 3.6.3 is shown the  $^{60}\text{Co}$  beta spectrum measured by one of the Si(Li) detectors, corrected for the detector response, from one of the permendure foil sources used in this experiment. There is no significant difference between

the spectra for the two sources used described in section 3.2. Compare with this the spectrum from a source deposited on a 200 micro g/ cm<sup>2</sup> Mylar backing shown in the same figure 3.6.3. Neglecting the scattering in the Mylar the difference in the spectra is attributed to scattering in the mendure foil. Here, it is assumed that the difference, the extra scattered beta particles, are completely depolarized. Thus, the expected transverse polarization of the beta particles that enter the polarimeter is that determined by the distribution of electrons from polarized 60-Co corrected by the simplified effects of scattering in the source foil.

The prediction of the transverse polarization measured by the polarimeter must be corrected for the deflection of the momentum and spin of the electrons in the magnetic field used to saturate the source foil. Mott scattering is sensitive to the transverse polarization of the electrons perpendicular to the scattering plane. For the accuracy needed here the quantum electrodynamical corrections to  $g = 2$ , the gyromagnetic ratio, for the electron can be ignored. Thus, the longitudinal polarization of the electrons will be constant. Therefore, the  $\vec{\sigma} \cdot \hat{p}$  terms in equation 3.6.2 will not contribute to the scattering asymmetries. The transverse polarization perpendicular to the scattering plane,  $P$  will be calculated by considering the two polarizations  $P_{||}$  and  $P_{\perp}$ . The polarization

$$P_{||} = \frac{\gamma m}{E} \frac{\langle J \rangle}{J}$$

is constant as the electron is deflected by the magnetic field. The polarization  $P_{\perp}$  which is the component perpendicular to  $\vec{J}$  and the momentum is

$$P_{\perp} = \frac{Zm}{E} \frac{\langle J \rangle}{J}$$

$P_{\perp}$  precesses about the the B field at the same rate as the momentum. Shown in figure 3.6.4 are the initial and final relationships of these directions. Using  $P_{||}$  and  $P_{\perp}$  at the scattering foil the  $P_S$  can be calculated

for all  $d\Omega_1$  and  $d\Omega_2$  solid angle elements. At each energy the resulting  $P_S$  is corrected for the relative depolarization in the source due to the contribution of the scattered unpolarized electrons discussed above.

### 3.7 COMPARISON OF RESULT TO PREDICTION

The energy spectrum of electrons scattered from the gold foil of the polarimeter detected in Si(Li) detector 1 can be calculated as

$$G_1(E, P_S) = G_{\text{polarization independent}} + G_{\text{polarization dependent}} N t \int dE' W(E') F(E, E') * \int d\Omega' \left( \int d\Omega'' \frac{1}{\sin \phi} \frac{d\sigma}{d\Omega''}(E') \left[ 1 - P_S(E') S_{\text{eff}}(E', \theta) \right] \right)$$

where the geometry is shown in figure 3.6.1 . Here, N is the number density of Au nuclei and t is the thickness of the scattering foil.  $W(E')$  is the energy spectrum of electrons entering the polarimeter from the source presented in section 3.6.  $F(E, E')$  is the energy spectrum response function of the Si(Li) detector proportional counter system .  $P_S(E')$  is the predicted transverse polarization of the electrons perpendicular to the scattering plane as a function of electron energy. The  $\frac{d\sigma}{d\Omega''}$  and  $S(\theta)_{\text{eff}}$  are the Mott scattering cross sections. The  $1/\sin(\phi)$  term corrects for the effective thickness of the foil for oblique incidence. As a first approximation, this correction is simply the square root of 2.

The total proportional counter gated count rate in Si(Li) detector 1 in an energy interval  $\Delta E$  centered at E is

$$R_1(E, \Delta E, P_S) = B_1(E, \Delta E, P_S) + \Gamma_1(E, \Delta E, P_S)$$

The gamma rate in this energy interval is  $\Gamma_1$  . Thus the change in measured asymmetries in the previous section can be calculated .

$$A(E, \Delta E) = \frac{R_1(E, \Delta E, P_S) - R_2(E, \Delta E, P_S) - \{R_1(E, \Delta E, 0) - R_2(E, \Delta E, 0)\}}{R_1(E, \Delta E, 0) + R_2(E, \Delta E, 0)}$$

The contribution to  $\Delta A$  from the change in gamma ray rates can be estimated by measuring  $\Delta A$  at high energy where  $W(E)$  is zero. From figure 3.5.7 in section 3.5 this is seen to be zero in the energy interval of 300 - 400 Kev for all four data runs. Thus, we will assume that the gamma rays only

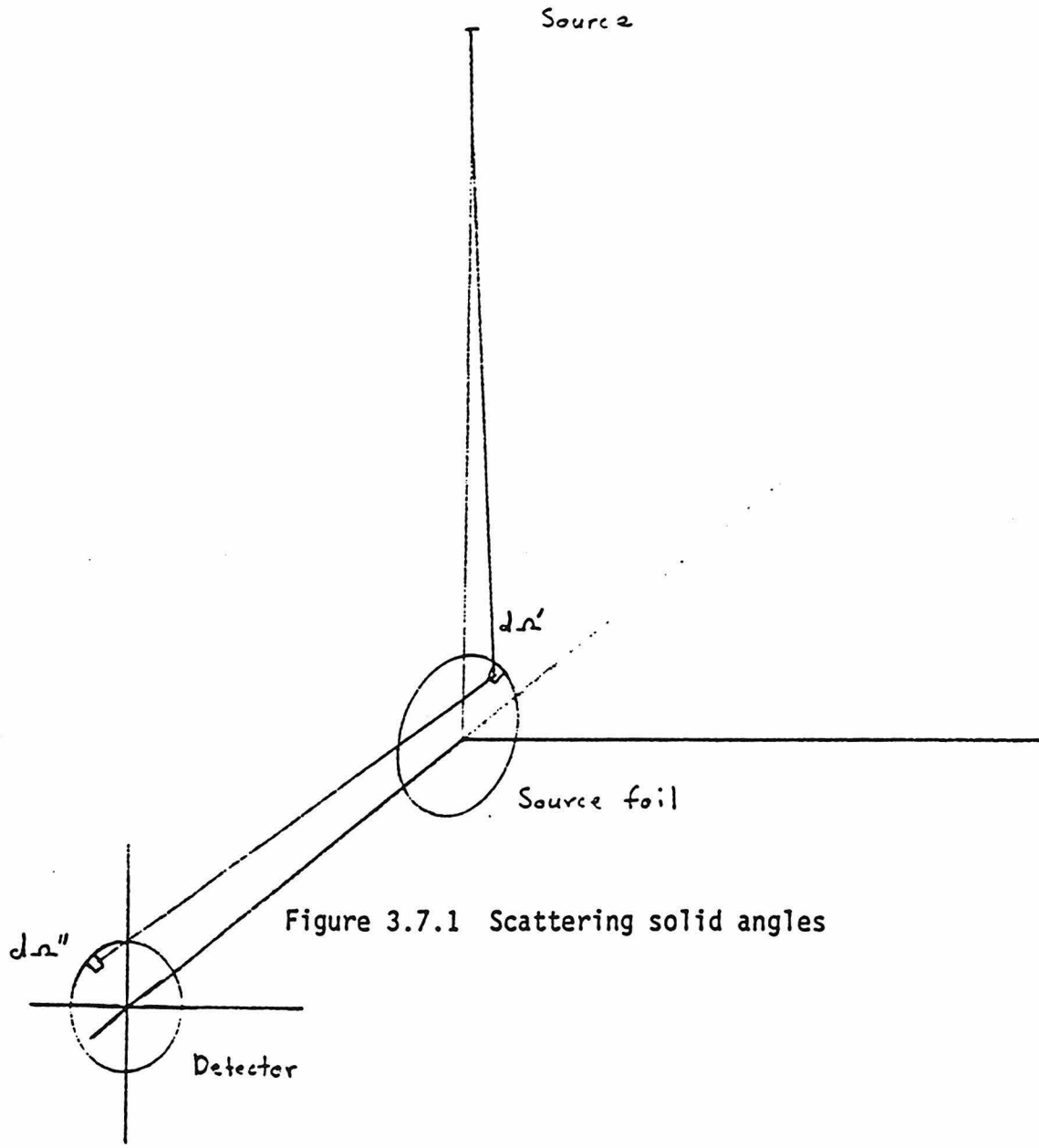


Figure 3.7.1 Scattering solid angles

affect  $\Delta A$  by their appearance in the denominator. This assumption will be discussed further in appendix A . Now, the  $\Delta A$  can be written

$$A(E, \Delta E) = \frac{\int dE \text{ } G_1 \text{ polarization dependent} - \int dE \text{ } G_2 \text{ polarization dependent}}{X_1(E, \Delta E) * B_1(E, \Delta E, 0) + X_2(E, \Delta E) * B_2(E, \Delta E, 0)}$$

where

$$X_1(E, \Delta E) = \frac{R_1(E, \Delta E, 0)}{B_1(E, \Delta E, 0)}$$

similarly for detector 2,

$$X_2(E, \Delta E) = \frac{R_2(E, \Delta E, 0)}{B_2(E, \Delta E, 0)}$$

are the measured ratios of total to beta rates shown in figure 3.7.2.

The energy response functions were measured using a 139-Ce source. A 200 micro Ci source on a 200 micro g / cm<sup>2</sup> Mylar backing was used in the polarimeter in a holder designed to place the source at the same position as the 60-Co sources when they are attached to the refrigerator. The measured spectra are shown in figure 3.7.3 . The total width of 25 keV of the K-conversion line energy peak is attributed to the constant 15 keV width of the Si(Li) detector plus the equally important widths due to energy loss straggling in the proportional counter and the variation in path length through the proportional counter. The width due to straggling is estimated to be about 15 keV for the K-conversion line. The remaining width due to path length variations of about 13 keV was taken to be constant as a percentage of energy loss in the proportional counter. The straggling width is expected to vary as the inverse of the velocity squared of the electrons. It is assumed that the height of the low energy tail relative to the peak height increases as the inverse of the kinetic energy of the peak toward low energy. With the

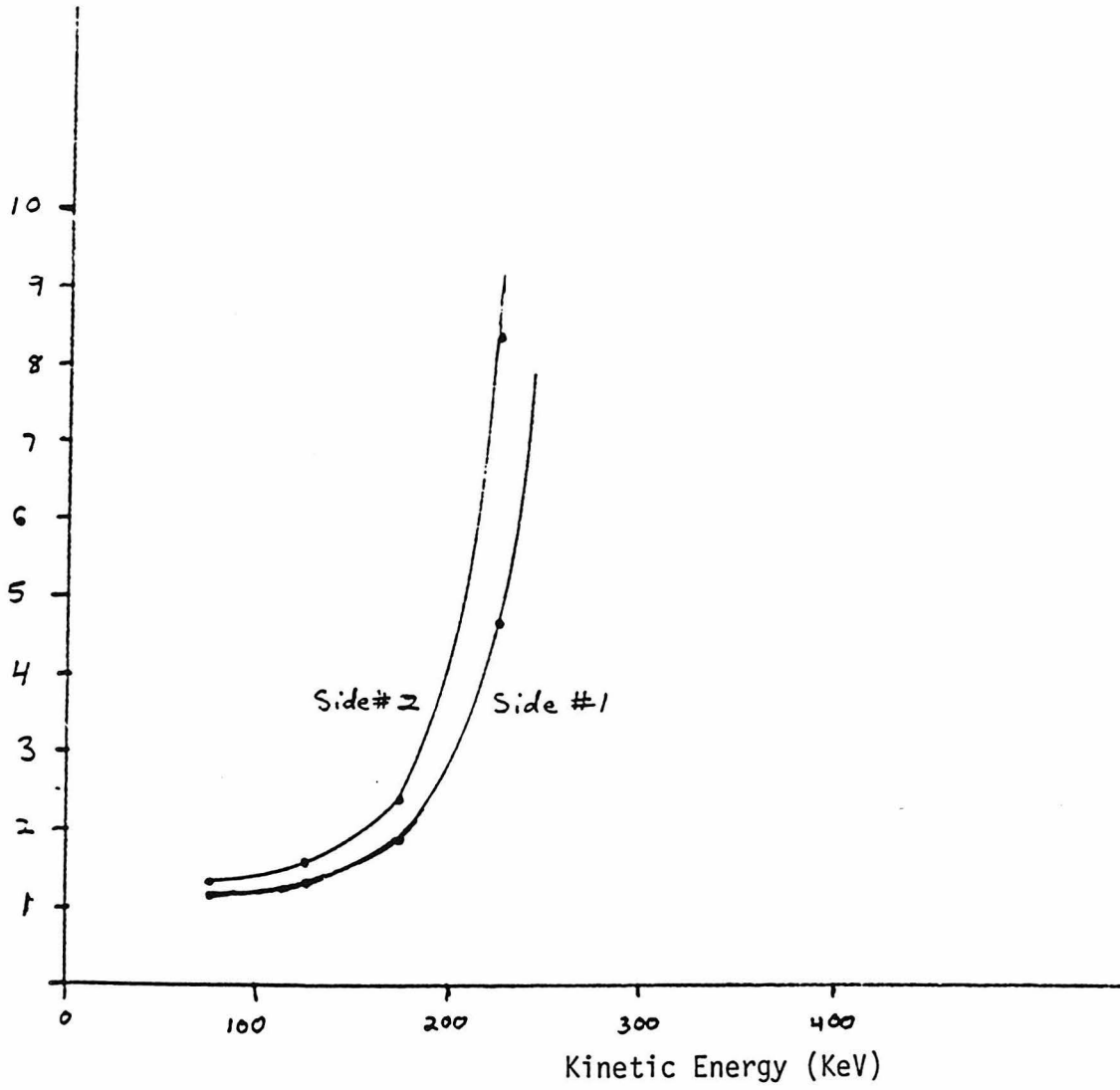


Figure 3.7.2 Ratio of total to beta particle counts in 50 keV intervals

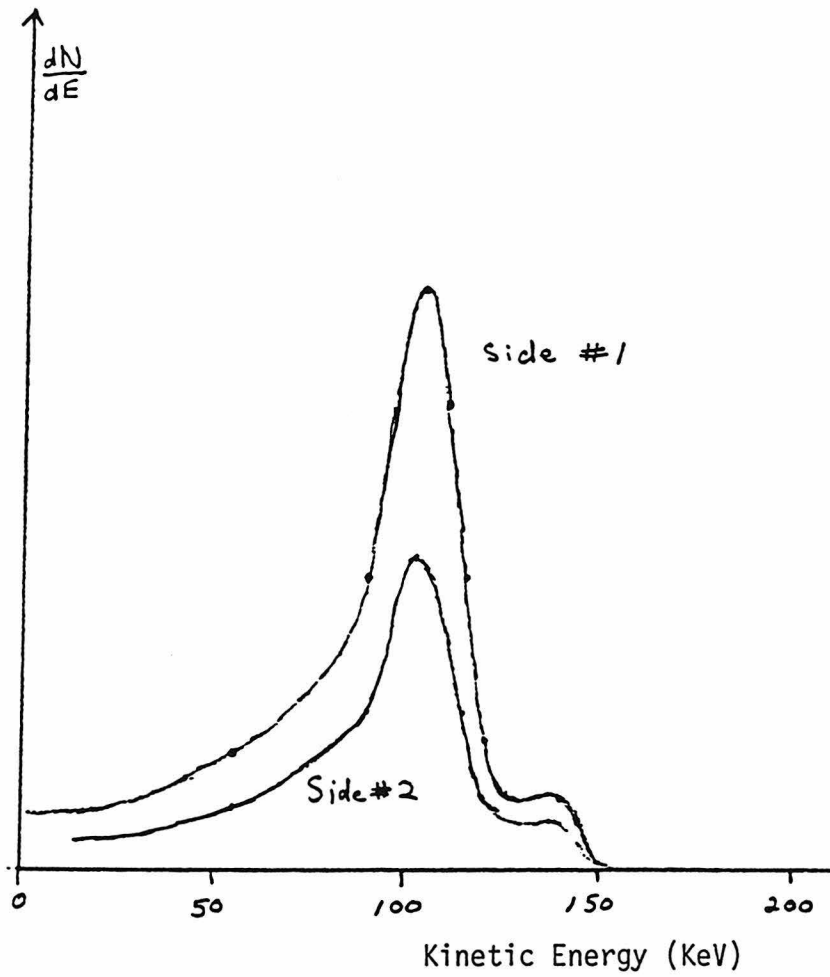


Figure 3.7.3 Response function of the polarimeter detector system

response function as a function of energy one can calculate the expected spectra for given Mott cross sections and input spectrum,  $W(E)$ .

The determination of the proper Mott cross sections to be used in equation 3.7.1 will be treated separately for the two sides of the polarimeter. The polarization independent cross sections to be used for scattering from finite thickness foils will be assumed to behave as

$$\frac{d\sigma}{d\Omega''} = \left( 1 + \frac{\alpha}{T} \right) \frac{d\sigma_p}{d\Omega''}$$

where  $\alpha$  is a constant and  $T$  is the kinetic energy of the electrons. Thus, at high energy the cross section becomes as expected the single scattering cross section,  $\frac{d\sigma}{d\Omega''}$ . For side two multiple scattering in the foil is expected to be minimal. The value,  $\alpha = 17$  keV is determined by fitting the calculated spectrum shape using  $\frac{d\sigma}{d\Omega''}$  in equation 3.7.1 to the measured spectrum shape of figure 3.5.2.

For side 1 the polarization independent cross section is changed much more by multiple scattering from the single scattering cross section. The geometry of the foil with respect to the incident electrons and the detectors allows multiple small angle scattering to mimic a single large angle scattering. The higher rate of scattered electrons from the 60-Co sources seen on side 1 as compared with side 2 is due to this increase in scattering in spite of the smaller total solid angle for scattering into side 1. It is assumed that the multiple scattering can be accounted for by the addition of a similar term in  $\frac{d\sigma}{d\Omega''}$  with  $\alpha = 115$  keV determined by the best fit to the measured scattered spectrum shape for the 60-Co sources. Thus, for side 1

$$\frac{d\sigma}{d\Omega''} = \frac{d\sigma_p}{d\Omega''} \left( 1 + \frac{\alpha}{T} \right)$$

The effective Sherman function,  $S_{eff}(\theta)$ , for side 2 was found by applying a correction to the theoretically predicted single scattering  $S(\theta)$  of Holzwarth and Meister.<sup>32</sup> It is used as  $S_{eff}(\theta) = \frac{S(\theta)}{1 + \delta(E) t}$

where  $t$  is the foil thickness and  $\delta$  is taken from the measurements of Van Klinken for the transmission geometry at 105 degrees. It is assumed that  $\delta$  does not vary over the scattering angles used in this polarimeter for side 2. Plotted in figure 3.7.4 is  $\delta$  as a function of energy for the foil thickness of 135 micro  $g/cm^2$  used in this experiment.

There have been no systematic studies of  $S(\theta)$  for reflection geometry which is used for side 1, see figure 3.6.4. Therefore, the analysis will be carried out using two different assumptions about the effects of multiple scattering on the  $S_{eff}(\theta)$  for side 1 of the polarimeter. These assumptions are that either i)  $S_{eff}(\theta) = S(\theta)$ , the effective Sherman function is not affected by the multiple scattering; or ii)  $S_{eff}(\theta) = \frac{S(\theta)}{1 + \alpha/T}$ , it is reduced by the multiple scattering. This second assumption can be understood by writing the cross section as

$$\frac{d\sigma}{d\Omega} = \frac{d\sigma}{d\Omega} \left( 1 + \frac{\alpha}{T} - P_S S_{eff}(\theta) \right)$$

where the increase in scattering due to multiple scattering only affects the polarization independent cross section. Thus, it is equivalent to a statement that multiple scattering contributes only to an increase in the background of polarization independent scattering. This may be justified by the idea that the multiple scattering is mainly small angle scattering where  $S(\theta)$  is near zero.

The  $\Delta A$  have been calculated for many energies of interest for the two assumptions above. Figure 3.7.5 shows  $\Delta A$  compared to the combined experimental results presented in section 3.5. The experimental results from runs 2 and 4 were combined with those for runs 1 and 3 with a relative minus sign because of reversed nuclear polarization direction in these runs. Since the expected  $\Delta A$  is proportional to  $\langle J \rangle / J$  the results in table 3.5.1 are used to combine the runs results.

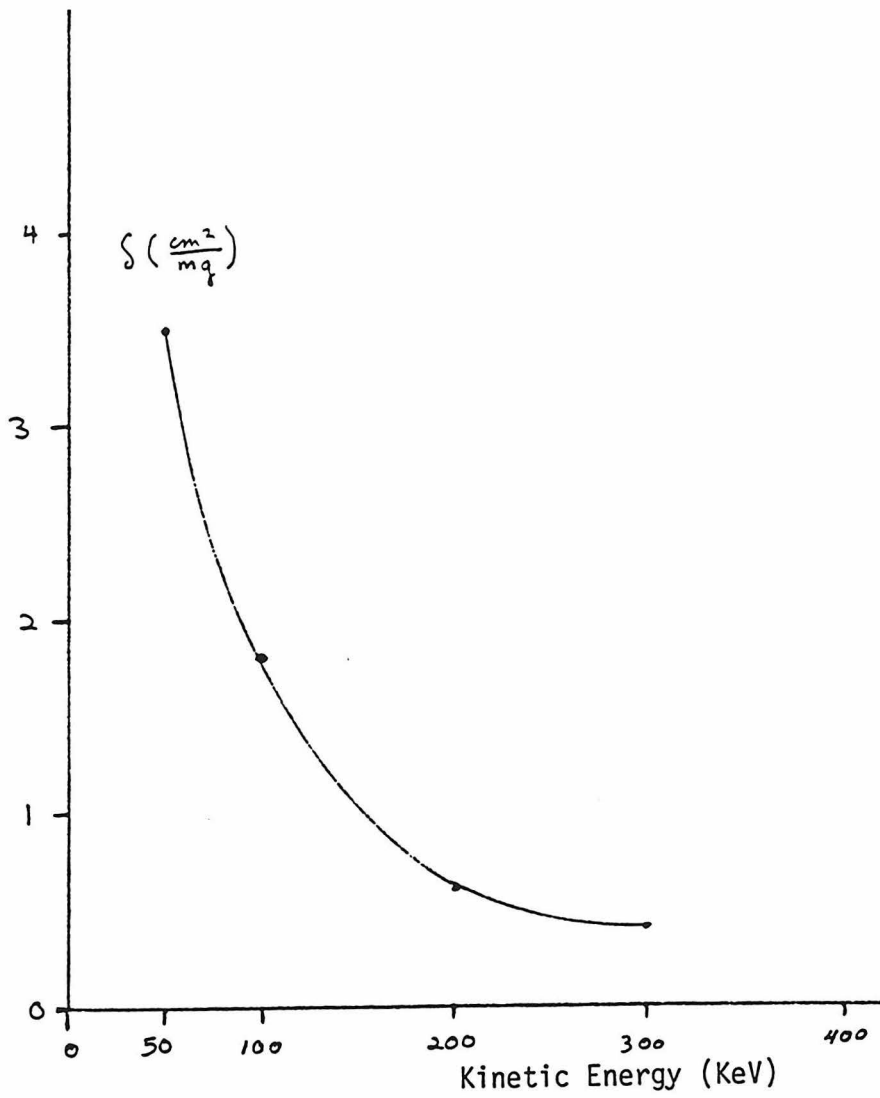


Figure 3.7.4 Finite foil thickness correction to polarization sensitivity

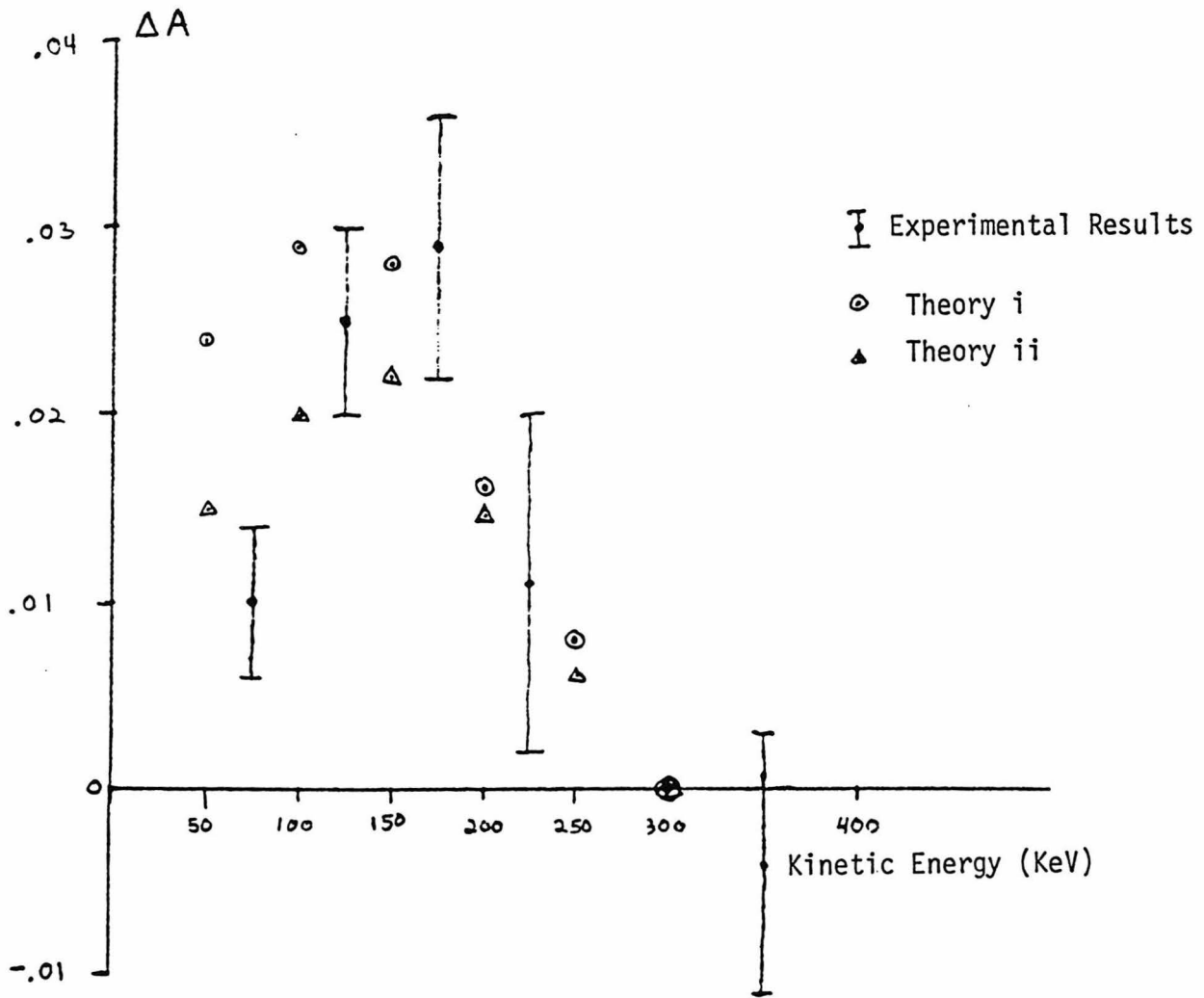


Figure 3.7.5 Measured  $\Delta A$  as a function of energy

The goal of this experiment is to verify the predictions of the beta decay theory. Therefore, the analysis was extended to determine the best experimental value for  $N$  of  $^{60}\text{Co}$  in equation 2.2.1 . The expected value for  $N$  is

$$\text{V - A Theory } N = \epsilon \frac{\gamma m}{E} ,$$

where  $\epsilon = 1$  for the theoretical prediction. The best fit of the predicted  $\Delta A$  to the experimental results using assumption ii described above between 100 and 250 Kev is with

$$\epsilon = 1.2 \pm 0.2$$

The results are consistent with the expected effect based on the theory of the transverse polarization of beta particles from the decay of oriented nuclei.

## Chapter 4 Discussion

### 4.1 MEASUREMENT OF R FOR 60 - CO

The goal of the experiments in our laboratory with polarized nuclei is a search for possible violations of time reversal symmetry in nuclear beta decay correlations. The immediate plan is to begin a measurement of the correlation term

$$R \vec{J}_{Co} \cdot \vec{p}_\beta \times \vec{\sigma}_\beta$$

for 60-Co. This is sensitive to  $C_T C_A \sin(\phi_{TA})$ .

A new source preparation technique appears possible which would much reduce the external magnetic field needed to polarize the source foil. It is possible that 60-Co can be diffused into a thin film( 50 Å thick ) of permendure. The demagnetizing field for such a foil is less than the coercivity of the permendure. Thus, the foil would become a switchable permanent magnet needing no external magnetic field to remain polarized. This new technique will be explored in the near future.

An experiment to measure R for 60-Co is expected to achieve a limit of

$$\left| \frac{C_T}{C_A} \right| \sin \phi_{TA} < 0.02$$

within a short time. The apparatus described above may be used to measure R and N correlation terms in 56-Co or other mixed Fermi-Gamow-Teller transitions. In these cases one might expect to observe 10% scalar contributions with 90 relative phase due to Higgs exchange mechanisms. The existence of such interactions cannot be ruled out by current experimental results. Such an expuriment may be persued in the future.

APPENDIX A CONTRIBUTIONS OF GAMMA RAY BACKGROUND

The total proportional counter gated count rate in Si(Li) detector 1 in an energy interval  $\Delta E$  centered at  $E$  is

$$R_1(E, \Delta E, P_S) = B_1(E, \Delta E, P_S) + \Gamma_1(E, \Delta E, P_S).$$

Thus, the measured change in asymmetries is

$$A(E, \Delta E) = \frac{R_1(E, \Delta E, P_S) - R_2(E, \Delta E, P_S) - \{R_1(E, \Delta E, 0) - R_2(E, \Delta E, 0)\}}{R_1(E, \Delta E, 0) + R_2(E, \Delta E, 0)}.$$

In section 3.7 the contributions from  $\Gamma_1$  and  $\Gamma_2$  are assumed to be small. Using the definitions

$$X_1(E, \Delta E) = \frac{R_1(E, \Delta E, 0)}{B_1(E, \Delta E, 0)}$$

for sides 1 and 2, the contribution to  $A$  from  $\Gamma$ 's becomes

$$A_\gamma(E, \Delta E) = \frac{\Gamma_1(E, \Delta E, P_S) - \Gamma_2(E, \Delta E, P_S) - (\Gamma_1(E, \Delta E, 0) - \Gamma_2(E, \Delta E, 0))}{\Gamma_1(E, \Delta E, 0) \frac{X_1(E, \Delta E)}{X_1(E, \Delta E) - 1} + \Gamma_2(E, \Delta E, 0) \frac{X_2(E, \Delta E)}{X_2(E, \Delta E) - 1}}.$$

Assuming  $\Gamma$  is due to gamma rays emitted at an angle of 90 degrees with respect to the polarization of the nuclei

$$\Gamma_{1,2}(E, \Delta E, P_S) \doteq 1.04 \Gamma_{1,2}(E, \Delta E, 0) \quad (A.2)$$

for all four data runs. In addition

$$|\Gamma_1(E, \Delta E, 0) - \Gamma_2(E, \Delta E, 0)| \leq 0.01 \quad (A.3)$$

in every energy interval. Using these conditions the asymmetry change is limited to

$$A_\gamma(E, E) \leq \frac{8 \times 10^{-4}}{\frac{X_1(E, E)}{X_1(E, E) - 1} + \frac{X_2(E, E)}{X_2(E, E) - 1}}. \quad (A.4)$$

In figure A.1  $A_\gamma$  is shown.  $A_\gamma$  is far smaller than the statistical errors in  $\Delta A$  of about 5% and thus can be neglected.

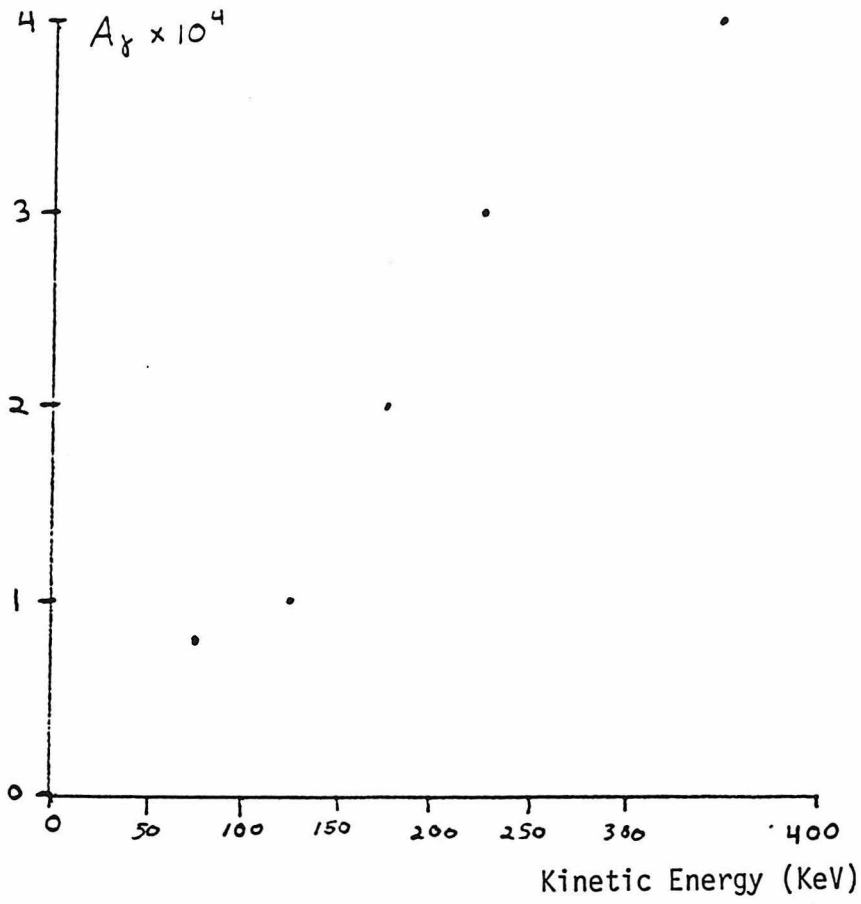


Figure A.1 Limit on contribution of gamma asymmetry

REFERENCES

1. Entenberg, A., et al. Phys. Rev. Lett. 42, 1198(1979)
2. Arnison, G., et al. Phys. Lett. 122B, 103(1983)
3. Weinberg, S., Phys. Rev. Lett. 19, 1264(1967)
4. Lee, T. and Yang, C. Phys. Rev. 104, 254(1956)
5. Christenson, J., et al. Phys. Rev. Lett. 13, 138(1964)
6. Kobayashi, M. and Maskawa, T. Prog. Theor. Phys. Japan 49, 652(1973)
7. Weinberg, S., Phys. Rev. Lett. 37, 657(1976)
8. Deshpande, N. and Ma, E. Phys Rev. D18, 2574(1978)
9. Jackson, J., et al. Phys. Rev. 106, 517(1957)
10. Boothroyd, A., et al. Phys. Rev. C 29, 603(1984)
11. Lobashov, V., et al. Neutrino 82, Lake Balaton
12. Commins, E. and Bucksbaum, P. Weak Interactions of Leptons  
Cambridge University Press; Cambridge(1983)
13. Deshpande, N., et al. Phys. Lett. B108, 42(1982)
14. Blanke, E. et al. to be published; private communication
15. Gimlett, J., et al., Phys. Rev. C 24, 620(1981)
16. Corriveau, F., et al., SIN Newsletter 12, 24(1979)
17. Wu, C., et al. Phys. Rev. 105, 1413(1957)
18. Steinberg, R., et al. Phys. Rev. Lett. 33, 41(1974)
19. Hallin, A., et al. Phys. Rev. Lett. 52, 337(1984)
20. Schneider, M., et al. Phys. Rev. Lett. 51, 1239(1983)
21. Calaprice, F., et al. Phys. Rev. C 15, 381(1977)
22. See Ref. 17
23. Mott, N. Proc. Roy.Soc. A124, 425(1929)
24. van Klinken, J. Nucl. Phys. 75, 145(1966)

25. van Klinken, J., et al., Phys. Rev. Lett. 50, 94(1983)
26. Tolhoek, H., and de Groot, A., Physica 17, 81(1951)
27. See Ref. 20
28. Steffen, R., and Alder, K., The Electromagnetic Interaction in Nuclear Spectroscopy, edited by Hamilton, North Holland;Amsterdam
29. Jackson, J. et al, Nuclear Physics 4, 206(1957)
30. Ullman, J., et al., Phys. Rev. 122, 536(1961)
31. See Ref. 24
32. Holzwarth, G. and Meister, H. Nuclear Physics 59, 56(1964)
33. Nuclear Data B2-5-55(1968)
34. Nuclear Data Sheets 16, 334(1975)
35. L. Chirovski, private communication
36. Bozorth, Ferromagnetism, D. van Nostrand;Princeton (1951)
37. Revell, R., et al., Brit. J. App. Phys. 6, 23(1955)
38. Scott, W., Phys. Rev. 76, 222(1949)